Data-Constrained Biophysical Modeling Of Human VIM To Assess Contributions Of Intrinsic Oscillatory Activity To Essential Tremor

Shane Lee[1,2], David J Segar[1,4], Wael F Asaad[1,2,3,5,6], Stephanie R Jones[1,2,7]

Brown University [1]Department of Neuroscience, [2]Carney Institute for Brain Science, [3]Alpert Medical School Department of Neurosurgery; [4]Brigham and Women's Hospital Department of Neurosurgery; [5]Rhode Island Hospital Department of Neurosurgery; [6]Norman Prince Neurosciences Institute; [7]Providence Veteran's Affairs Medical Center, Center for Neurorestoration and Neurotechnology

Corresponding Author:

Shane Lee
Brown University
Department of Neuroscience
185 Meeting St Box GL-N
Providence RI 02912

shane_lee@brown.edu

Abstract

Essential tremor (ET) is the most common movement disorder, in which the primary symptom is a prominent, involuntary 4–10 Hz rhythmic movement. The presence of tremor frequency activity in the ventral intermediate nucleus of the thalamus (VIM) is well established, but it is often assumed that it is driven by cerebellar tremor frequency activity, while the role of intrinsic oscillatory activity in VIM is not clear. An improved understanding of the mechanisms of tremor and non-tremor activity in the VIM may lead to better pharmacological and neuromodulatory therapies. We recorded local field activity during tremor in the VIM from 5 patients during deep brain electrode implantation surgery to constrain a biophysically-principled computational model of tremor field activity in the VIM, coupled with the thalamic reticular nucleus (TRN). We compared tremor frequency activity in the model generated either by extrinsic tremor-periodic drive or by intrinsic VIM-TRN interaction. Extrinsic and intrinsic tremor frequency oscillations in the model depended on T-type Ca^{2+} channels in different ways. Both also depended on GABA modulation in a site- and type-specific manner. These results suggested that efficacy of pharmacological manipulations may depend upon the mechanisms generating tremor activity in VIM. Simulated non-tremor-related cerebellar drive decreased extrinsic tremor activity but increased intrinsic tremor activity. Intrinsic tremor power was increased with an external tremor frequency drive, suggesting that both mechanisms may be important to understand the emergence and cessation of tremor activity in VIM. Our results lead to experimentally testable predictions on modulating tremor frequency activity that can help to improve future treatment strategies for ET.

Significance Statement

Essential Tremor (ET) is a movement disorder in which the primary symptom is a prominent, involuntary, and rhythmic shaking, often of the arms. Electrical activity in many areas of the brain exhibit rhythmicity that is related to the patient's tremor. One such area resides in a brain structure called the thalamus, but it is not fully known what gives rise to the tremor-related activity. Here, we recorded electrical activity from the thalamus in ET patients and created a computational model of this activity in the thalamus. Model results suggest how to differentiate tremor mechanisms and how these differences may contribute to other impairments in ET. Knowledge of the biophysical mechanisms contributing to tremor can ultimately lead to improvements in treatments to improve symptoms of ET.

Contents

1 Introduction **6**

2 Methods **7**

2.1 VIM local field potential activity during tremor in ET 7

2.2 Overview of the model network 8

2.3 Thalamocortical VIM Cells 9

2.4 Thalamic Reticular Nuclear Cells 11

2.5 Synapses 12

2.6 Additional Inputs 12

2.7 Numerics, outputs, and analysis 13

3 Results **15**

3.1 Local field potentials in VIM showed tremor frequency activity correlated with tremulous movement 15

3.2 Dual mechanisms in VIM-TRN model led to tremor frequency activity . . . 15

3.3 Tremor frequency activity depended on T-type Ca^{2+} in VIM cells 16

3.4 Tremor frequency power depended upon $GABA_A$ within the TRN but not from TRN to VIM 18

3.5 Tremor frequency power was reduced with reductions in $GABA_B$ conductance in both models 19

3.6 Intrinsic tremor frequency activity was further increased by tremor periodic input 19

3.7 Simulated non-tremor frequency activity reduced tremor power in extrinsic network but increased tremor power in intrinsic network 20

4 Discussion **21**

4.1 Origins of tremor frequency activity in VIM 21

4.2 Non-tremor cerebellar inputs may exacerbate tremor in VIM 22

4.3 Broad effects of GABA modulation on tremor frequency activity in VIM . . 23

4.4 T-type Ca^{2+} currents affected tremor frequency activity in VIM models . . 24

List of Tables

1 Key parameters compared to original model 35
2 Modulation of tremor frequency activity by T-type Ca^{2+}Conductance in models 36
3 Modulation of tremor frequency power by GABA Conductance in models . 37
4 Modulation of tremor frequency power by synaptic inputs in models . . . 38

List of Figures

1 Significant VIM tremor frequency activity during physiological tremor . . 39
2 Model VIM-TRN networks 40
3 Model cells replicate original models 41
4 Field examples of recorded tremor frequency oscillations in VIM data and in model 42
5 Extrinsic and intrinsic models of tremor frequency oscillations showed similar properties 43
6 Changes in T-type Ca^{2+} conductance affect both extrinsic and intrinsic tremor frequency activity 44
7 Tremor frequency power varied by GABA type in both models 45
8 Intrinsic network tremor frequency power increased with tremor-phasic input 46
9 Non-tremor frequency inputs increased intrinsic but not extrinsic tremor frequency activity 47

1 Introduction

Essential Tremor (ET) is the most common movement disorder in adults, affecting 5–6% of the population [39, 40]. ET is dominated by a low frequency (4–10 Hz), involuntary "intention" tremor, often of the upper limbs [17, 40], but is no longer considered a monosymptomatic disorder [36], and both motor and cognitive symptoms have been observed [35, 41, 62]. Potential cerebellar dysfunction has been implicated in the etiology of ET [13, 17, 18, 41, 64], though the pathophysiology is heterogeneous and not fully understood [11, 21, 41, 54]. Tremor, by far the most dominant symptom, has been associated with tremor frequency oscillatory neural activity in the thalamus [29, 33, 58], primary motor cortex [24, 25], cerebellar cortex [58], and brainstem [58]. It remains unclear though unlikely that there is a single driver of tremor frequency activity [11, 54].

An improved understanding of the cellular and circuit mechanisms generating tremor frequency neural activity in ET may lead to more effective pharmacological or electrical treatments. Prior computational modeling has investigated multiple aspects of the timing of deep brain stimulation on thalamic cells, including rebound bursting [7, 10, 36, 65], and recent work investigated mean field tremor activity in thalamus [70]. Yet to our knowledge, within the VIM, whether tremor frequency neural activity is intrinsically or extrinsically modulated has not been fully established and is essential to improving treatment strategies.

Here, we recorded tremor frequency field activity from VIM in 5 ET patients to constrain a biophysically-principled computational model of tremor activity in the VIM, containing multi-compartment Hodgkin-Huxley-type neurons and based on a canonical model of thalamic oscillatory activity that involves reciprocal interaction with the thalamic reticular nucleus (TRN) [14]. We compared the recordings to both extrinsically generated and intrinsically generated tremor frequency oscillations in the model. T-type Ca^{2+} channels are hypothesized to be involved in tremorgenic oscillatory activity [31] and more broadly involved in oscillatory activity within the thalamus [14, 16], so T-type Ca^{2+} currents were varied in the models. Additionally, GABA-ergic modulation was varied in the model, as it has been implicated in multiple aspects of tremorgenic oscillatory activity, particularly in the cerebellum [19, 42] but also within the VIM [1, 8, 19].

Our goal was to assess the extent to which intrinsic versus extrinsic mechanisms may contribute to tremor and how differences in these networks respond differently to afferent inputs and pharmacological manipulations.

2 Methods

2.1 VIM local field potential activity during tremor in ET

We recorded microelectrode and behavioral data intraoperatively during deep brain stimulation (DBS) lead implant surgery performed by WFA, with the approval of the Lifespan/Rhode Island Hospital Institutional Review Board. All patients provided written informed consent. During the routine intraoperative microelectrode recording, in most cases 3 (but up to 4) microelectrodes were placed in the VIM. Neural data were recorded at 40 kHz through a Guideline 4000 LP+ (FHC, Bowdoin, ME, USA), downsampled to 1 kHz, and sent to a neural data acquisition system (Plexon, Dallas, TX, USA).

With electrodes in the VIM, patients performed a center-out joystick task programmed in MonkeyLogic [2, 3] and displayed on a computer monitor. In this task, a target appeared on the screen at one of eight locations positioned equally around an imaginary circle. Patients moved a cursor controlled by the joystick to the target and held at the target for 500 ms. Patients performed 100–160 trials of this task.

MonkeyLogic and joystick data acquisition were controlled by standard computer hardware. Joystick data were acquired through data acquisition boards from National Instruments (Austin, TX, USA), which were also used to send digital event codes to synchronize with the neural data.

The joystick-controlled on-screen cursor deflection from the origin was captured in both x and y directions (arbitrary units, Fig. 1A–B). These signals were filtered in the tremor frequency band (4–10 Hz), and the Hilbert transform was used to determine the envelope of the tremor activity. The joystick aggregate represented the Euclidean norm of the x and y components (Fig. 1C). An identical analysis was performed on each field recording from the VIM (Fig. 1D).

For each trial, 1 second epochs of both the aggregate joystick envelope (Fig. 1E) and the field envelope (Fig. 1F) were calculated starting from the end of each trial. The envelopes for both in each bin were averaged (horizontal lines) and represented a single pair of data. For each electrode, the Pearson's correlation coefficient was calculated between the joystick envelope and the field envelope in the tremor band. An example from one electrode is shown in Fig. 1G.

To assess significance, we ran a Benjamini-Hochberg test [6] for all calculated joystick-field correlations with a false positive rate (q) of 0.05 and a p-value threshold of 0.05. Significant correlation occurred when tremor power in the joystick and tremor power in the field increased concurrently.

For all electrodes showing significant correlation to the tremor, the top half of mean tremor magnitudes were used to select corresponding raw fields (Fig. 1H). Spectral power of the field epochs was calculated using the same discrete Fourier method as above. The power spectra were averaged, and the standard error was calculated, as represented in Fig. 1I.

2.2 Overview of the model network

We sought to understand the biophysical cellular and circuit level contributions to tremor frequency neural activity in VIM. We used NEURON 7.5 [12, 27] to simulate a small volume of VIM—which might be considered a tremor cluster [51]—consisting of 25 multicompartmental thalamocortical VIM relay cells and 25 multicompartmental thalamic reticular nuclear (TRN) cells (Fig. 2). The basic network was based on prior modeling of networks of thalamocortical relay cells [16] and thalamic reticular network cells based on electrophysiological recording of ferret thalamus [14–16]. Bursting VIM cells, a prominent feature in ET [29], were also featured in these models. Though the original work was a model of sleep or anesthesia, bursting modes underlying oscillatory activity have also been shown to be important in normal function [60], and we hypothesized that similar mechanisms may underlie pathological VIM bursting.

We compared properties of the network for two possible mechanisms of tremor frequency oscillations: extrinsic and intrinsic (Fig. 2A–B). In both networks, VIM cells created AMPA-ergic synaptic connections with the TRN cells, and TRN cells created both $GABA_A$ and $GABA_B$ connections with the VIM cells. TRN-TRN $GABA_A$ connections were also created reciprocally.

VIM cells (outlined in detail below) in the extrinsic model were driven by a tonic applied current of 0.06 nA to mimic the thalamic "tonic" mode that did not auto-generate oscillations [60] but responded to tremor-frequency AMPA-ergic synaptic inputs faithfully. A phasic input with a mean frequency of 6 Hz drove activity in this network. The input was initiated at 50 ms, and on each cycle of the input, 30 synaptic inputs were simulated with a Gaussian temporal distribution (σ=20 ms) and unitary weights of 4.25×10^{-3} μS.

In the intrinsic model, oscillations generated in the tremor frequency range were based on reciprocal interactions between the VIM and TRN cells. The intrinsic model had no tremor-frequency synaptic drive.

VIM cells were chosen from a uniform spherical distribution centered about the origin, with a cell density of approximately 15,000 cells per mm^3 [28] (Fig. 2C–D). The volume of VIM cells simulated was approximately 2.5 mm away from the shell of TRN along an x-axis (arbitrarily chosen), based on the overall size of VIM estimated at 5 x 4

x (0.5–3) mm^3 [20].

The 25 TRN cells (outlined in detail below) were assumed to be near the VIM cells, and their axons were projected directly into the volume of VIM. The TRN somata were also uniformly distributed but throughout a volume spanning the circumference of the VIM sphere in two dimensions, with a TRN depth of 1 mm (approximated from [31]).

2.3 Thalamocortical VIM Cells

2.3.1 Geometry and Biophysics

The thalamocortical VIM cells were modeled using Hodgkin-Huxley dynamics after the 3-compartment cell from Destexhe [16]. In general, cell membrane voltages v_i for compartment i were given by the form of Eqn. 1, a sum of ionic, adjacent compartmental, synaptic (I_{syn}), and external input ($I_{external}$) currents. Ohmic currents were a function of the compartmental voltage and the reversal potential E_{rev} for a particular ionic species.

$$\begin{aligned} \dot{v}_i &= -\sum_{ion} I_i - I_{i-1} - I_{i+1} + I_{syn} + I_{external} \\ I &= g(v) \cdot (v - E_{rev}) \end{aligned} \tag{1}$$

The original cell included a soma and a dendritic branch that consisted of two compartments. We adapted this model in several ways, summarized in Table 1A–B. First, we reduced the volume of the somatic compartment to conform to estimates of the size of human VIM cells [28]. Second, we included two more dendritic branches, radially outward from the soma, to reflect the stellate-like nature of these cells [28], and we included an axonal compartment. The VIM cells included all currents from the original model (Na^+, K^+, T-type Ca^{2+}, and passive leak) and also included an additional potassium leak channel to sustain intrinsic T-type Ca^{2+}-mediated oscillations in the VIM cells [14].

The biophysics were subsequently tuned to mimic the dynamical properties of the original cell (Table 1B). In particular, the original thalamocortical cell somata had a cylindrical surface area of approximately 3138 μm^2, larger than estimates in VIM of 500–900 μm^2 [28]. Therefore we reduced the cylindrical surface area to 899 μm^2.

We added two additional dendritic branches compared to the original model, totaling three dendritic branches, each consisting of two compartments. The dendrites were arranged in the xy-plane for simplicity but at different angles: $\pi/4$, $3\pi/4$, and -$3\pi/4$ radians (see Fig. 2C–D). For each dendrite, the diameters and lengths from the

original model were preserved (Table 1).

Axonal biophysical parameters were adapted from prior modeling work [46] and adapted to enable axonal spiking to follow somatic output. The axon was 2.5 mm in length, oriented along the +x axis, with a diameter of 2 μm and was unmyelinated, unlike previous work.

In some simulations, the T-type Ca^{2+} permeability (ρ_{TCa}, in the soma and dendrites) was varied for all compartments simultaneously by a scaling factor S_{Ca} that scaled the permeability of each compartment's default value (listed in Table 1B). At baseline, S_{Ca} was 5.1. For simulations in which S_{Ca} was changed, values are reported relative to this baseline; for example, a relative value of 0.5 corresponds to a S_{Ca} value of 2.55.

2.3.2 Noisy background inputs

For all VIM cells, a Poisson-distributed background synaptic input was also included to give a baseline, non-tonic level of excitation to the network. The rate parameter λ was 10 ms, with a fixed strength of 5×10^{-3} μS. For all VIM and TRN cells, total number of segments in each compartment was set to 1 segment per 100 μm. One-third of cells also received -0.01 nA, due to estimates of the number of thalamic cells showing tremor activity [29], and one-half of the remaining cells arbitrarily received 0.05 nA for heterogeneity, but neither of these modifications made substantial changes in the spiking activity of the cells (data not shown).

2.3.3 VIM cell replicated original thalamocortical cell properties

The dynamical behavior of the original thalamocortical cell was preserved in the modified VIM cell (Fig. 3A). The original thalamocortical cell (Left panel of Fig. 3A) was simulated for 1.5 s, with the temperature parameter in NEURON set to 36°C. In the present VIM cell (Right panel of Fig. 3A), the initial membrane potential for all compartments was chosen from a Gaussian distribution with a mean of -85 mV and a standard deviation of 2 mV.

Upon running the simulations, a short burst of spikes were elicited before returning to a steady state membrane potential of -74 mV. Two tonic current clamp stimulations were then applied. At 0.4 s (first green line in Fig. 3A), for 0.2 s, the stimulation amplitude was 0.07 nA in the original model and 0.17 nA in the VIM cell, which elicited two action potentials in each model. Upon release of the stimulation, the cells returned to baseline. At 0.8 s (second green line in Fig. 3A), for 0.2 s, the -0.10 nA were applied to both the original and new VIM cells. When this stimulation was released, a burst of action potentials mediated by T-type Ca^{2+} currents was elicited before the

membrane potential returned to baseline.

2.4 Thalamic Reticular Nuclear Cells

2.4.1 Geometry and Biophysics

The TRN cells were also modeled after 3-compartment cells from Destexhe [15]. The original cell included a soma and a dendritic branch that consisted of two compartments. Similar to the VIM cell, we used the same generic formulation as Eqn. 1 and adapted the original TRN model in several ways. Though the soma and dendrite were unchanged from the original TRN cell model, an additional dendritic branch—nearly identical to the original—was added to reflect lateral branching of cells through the TRN [52]. The dendritic arbor for each cell extended laterally within the model TRN, at opposite ends of the soma, at $\pi/2$ and -$\pi/2$, oriented within the TRN and perpendicular to the axonal projection to the VIM (see Fig. 2C–D). An unmyelinated axon was also added following prior work [46], with a length of 2.8 mm, oriented in the -x direction, and with a diameter of 2 μm. The same channels were inserted in the soma and dendritic sections: passive, Na^+, K^+, Ca^{2+} decay, and the original T-type Ca^{2+} channel [15]. A comparison of parameters is shown in Table 1A and 1C.

2.4.2 Noisy Background Inputs

All TRN cells also had a Poisson-distributed background AMPA-ergic synaptic input that contacted one distal dendritic compartment with a λ of 10 ms and a fixed strength of 5×10^{-3} μS, identical to that given to the VIM cells. One-quarter of cells randomly received 0.025 nA for heterogeneity.

2.4.3 TRN cell replicated original TRN cell properties

Similar to the VIM cell, we simulated the original cell TRN under a variety of conditions and matched that behavior qualitatively (Fig. 3B). The original TRN cell (Left panel of Fig. 3B) and the new TRN cell (Right panel of Fig. 3B) were simulated for 1.5 s. The initial membrane potential for all compartments in the new TRN cell was chosen from a Gaussian distribution with a mean of -65 mV and a standard deviation of 2 mV. At 0.1 s (first green line in Fig. 3B), for 0.1 s, the stimulation amplitude was set to -0.4 nA in the original cell and -0.68 nA in the new TRN cell. Release of the current clamp did not result in rebound depolarization. After the membrane potential stabilized, at 0.6 s, the cell was clamped at the same amplitude for twice as long—0.2 s, which resulted in a burst of spikes following the release. At 1.2 s, a positive current of

0.1 nA to the original cell and 0.15 nA to the new TRN cell resulted in tonic spiking for the entire 0.2 s. The cells returned to a baseline of -67 mV.

2.5 Synapses

Following the original network model of thalamus [14], the following synapses were included in this model: fast excitatory AMPA-ergic from VIM to TRN, fast and slow inhibition from TRN to VIM, and fast inhibition from TRN to TRN. Fast inhibition approximated $GABA_A$ in the model, while slow inhibition was a model for $GABA_B$. As a simplification from the prior model, synaptic currents were modeled with a two-state kinetic scheme of summed exponentials (Eqn. 2–3) [12], were created all-to-all, and there were no autapses.

$$I_{syn} = G \cdot (v - E_{rev}) \tag{2}$$

$$G = \bar{g} \cdot (e^{-t/\tau_2} - e^{-t/\tau_1}) \tag{3}$$

Conductances between VIM and TRN synaptic connections were set to generate tremor frequency activity in the intrinsic network (all units are μS): VIM-TRN AMPA conductance was 3.75×10^{-4}; the TRN-VIM $GABA_A$ conductance was 2.5×10^{-5}, the TRN-VIM $GABA_B$ conductance was 1.5×10^{-4}, the TRN-TRN $GABA_A$ conductance was 5×10^{-4}. These conductance parameters were the same for both networks.

The excitatory AMPA receptors had a reversal potential of 0 mV, an exponential rise time τ_1 of 0.5 ms, and an exponential decay time τ_2 of 2 ms. $GABA_A$ connections were modeled with τ_1 of 0.5 ms, τ_2 of 5 ms [32], and a Cl^- reversal potential of -85 mV. $GABA_B$ connections had a τ_1 of 1 ms, a τ_2 of 100 ms, and a K^+ reversal potential of -95 mV [14].

2.6 Additional Inputs

Aside from tonic currents and Poisson-distributed inputs applied to individual cells in the model (see above), externally sourced synaptic inputs were also simulated. To model ongoing, non-tremor inputs that might arise from cerebellum or cortex [36], we simulated additional Poisson-distributed inputs that terminated on AMPA-ergic synapses on the dendrites of the VIM cells. Each event time of the Poisson input consisted of 25 Gaussian-distributed inputs with a 3 ms standard deviation. The mean Poisson rate, at 40 sp/s, was within observed estimates of tonic spiking activity in the dentate nucleus [67]. The amplitude of the unitary input conductance was varied.

For the intrinsic network, we also simulated the effect of an external tremor-frequency input, modeled with an AMPA-like synaptic input that had an mean

interevent interval of ~167 ms (6 Hz). On each cycle of the input, 30 Gaussian-distributed inputs arrived at the distal end of a dendritic branch with a standard deviation of 20 ms. The amplitude of this conductance was also varied.

2.7 Numerics, outputs, and analysis

A step size of 0.025 ms was used for all simulations, and 10 iterations were run for comparison across noise conditions. Sources of noise in the model included the specific realizations of the uniformly-distributed spatial locations of the somata for both the VIM and TRN cells, the Gaussian initial membrane potentials, and the Poisson inputs. For most comparisons unless otherwise noted, a non-parametric Mann-Whitney U test was used to assess significance [44, 68], which for all simulations was defined as $p < 0.025$ (n=10 simulations for all comparisons unless otherwise noted). Analyses were performed in Python 3.5 with standard modules, SciPy 0.18, and NumPy 1.13.

We were primarily interested in how tremor periodic activity in VIM would transfer to downstream areas such as primary motor cortex, so the principal output analyzed in the model was the axonal output spiking from the VIM cells. Individual spikes were identified as the membrane potential crossed a 0 mV threshold. Spike times from all VIM cells were concatenated, and the aggregate spike output was convolved with a Gaussian window with a width of 10 ms and a standard deviation of 2 ms. Mean VIM spike outputs were calculated among different simulations. All error is represented as standard error, with the number of samples specified.

For comparison with neural recordings, local field potentials were also simulated, using the extracellular mechanism in NEURON. The virtual recording electrode was placed in the volume at coordinates (1250 μm, 1000 μm, 0 μm), as seen in Fig. 2C–D.

Spectral analysis was performed on the convolved spike output and also on the simulated field potential, using a standard discrete Fourier transform in which the frequency domain signal was represented as a density of the total signal energy. Tremor energy was calculated as the concentration of total energy in the tremor frequency band (4–10 Hz), enabling comparisons across conditions.

For analyses comparing extrinsic to intrinsic tremor power, all values were directly compared across conditions for statistical tests. Some values were reported relative to a baseline condition for convenience, which was established by taking the mean of the baseline condition and normalizing all compared values to that value. Statistical tests were not performed directly on normalized values.

Code accessibility

The model is available on ModelDB (https://senselab.med.yale.edu/ModelDB/) with accession number 240113.

3 Results

3.1 Local field potentials in VIM showed tremor frequency activity correlated with tremulous movement

Tremor frequency spiking activity and field activity are commonly observed features in the VIM [29, 50, 59]. To constrain field features in the model, we sought to understand properties of ongoing local field potential activity in VIM during tremulous movements from raw data. We recorded local field potentials at 44 microelectrode sites from 5 subjects during DBS electrode implant surgery (Fig. 1). Movement from the dominant arm was simultaneously recorded while the subjects manipulated a joystick that moved a cursor on a screen (see Methods). Tremulous movements were visibly captured (Fig. 1A–C). We calculated 1 second epochs of time-locked movement and VIM activity at each site and calculated the correlation of tremor frequency (4–10 Hz) power in both. Thirty-six of the 44 electrode sites showed significant correlation (example Fig. 1G). We took the strongest half of tremor movements by magnitude and calculated the power spectrum of the corresponding local field potentials (Fig. 1H). Among these fields, the peak spectral power occurred at 5.9 Hz (Fig. 1I), consistent with previous reports for activity in VIM [29, 30].

3.2 Dual mechanisms in VIM-TRN model led to tremor frequency activity

We sought to understand the role of cellular and circuit biophysics in the generation of tremor frequency local field potentials in the canonical thalamic circuit and the impact of these mechanisms on non-tremor-related motor activity. We modeled two potential mechanisms of tremor frequency oscillations in the thalamus: extrinsically driven and intrinsically generated (Fig. 2A–B). Though it is suggested that extrinsic cerebellar inputs drive tremor in thalamus [19, 41, 58], the intrinsic oscillatory capability of the thalamus is also well-described [14, 60], and we reasoned that the biophysical mechanisms underlying the intrinsic bursting mode of VIM may influence how tremor frequency activity is represented, which has implications for reduction of tremor. Complete details of the networks can be found in the Methods.

Both the extrinsic and the intrinsic models consisted of reciprocally connected ventral intermediate nucleus of the thalamus (VIM) and the inhibitory thalamic reticular nucleus (TRN) that exhibited tremor frequency oscillations consistent with our recordings. All simulations included 25 VIM cells, coupled all-to-all to 25 TRN cells. An example schematic geometry of the network is shown in Fig. 2C–D. Individual VIM and TRN cells in the model were modified from prior work [14–16] by adding compartments and tuning the biophysics to exhibit similar behavior under a range of

conditions (Fig. 3). We analyzed spike rate outputs at the distal axon terminal of the VIM cells to understand how tremor frequency activity in VIM might be transmitted to downstream areas such as primary motor cortex. The extracellular field potential was also simulated for comparison with the recordings.

Parameters in the model network were tuned to resemble the tremor frequency characteristics of our recordings during the strong tremor oscillatory fields (Fig. 4). The extrinsic 50-cell model exhibited tremor frequency activity generated with a tremor-periodic AMPA-like synaptic input into tonically activated VIM cells (Fig. 2A and Fig. 5A–E). Here the peak frequency occurred at 6.4 Hz, and the tremor frequency concentration was $0.571 \pm 0.018\ mV^2/\text{Hz}$. The intrinsic 50-cell model was generated through the reciprocal interaction of GABA-ergic inhibition from TRN and T-type Ca^{2+} currents in the VIM cells, with a peak frequency of 6.7 Hz and a tremor frequency concentration of $0.572 \pm 0.032\ mV^2/\text{Hz}$ (Fig. 2B and Fig. 5F–J). The tremor frequency power for the extrinsic and intrinsic models were not significantly different ($p = 0.45$).

VIM cell spike rates for both the extrinsic (35.5 ± 0.5 spikes/s) and intrinsic models (35.1 ± 0.39 spikes/s) were not significantly different ($p = 0.29$, Fig. 5D, I). Both were slightly higher than observed rates of 26.8 ± 5.3 spikes/s reported during behavioral tremor [30].

Overall, high amplitude fields strongly correlated to tremulous movements exhibited activity in the tremor frequency band (Fig. 4 and see spectrum in Fig. 1I), and the activity generated by the extrinsic and intrinsic models also exhibited visible tremor frequency oscillations (Fig. 5), though smaller in amplitude due to the size of the network (Fig. 4).

3.3 Tremor frequency activity depended on T-type Ca^{2+} in VIM cells

Prior work in the thalamus has shown the importance T-type Ca^{2+} channels for pacing oscillatory activity [14]. Therefore, we hypothesized that these channels may also be important in sustaining pathological, tremor frequency activity. We varied the T-type Ca^{2+} conductance simultaneously in multiple compartments in VIM cells using a scale factor (S_{Ca}) in both the extrinsic and intrinsic models and analyzed changes both in frequency and power (Fig. 6). Changes to S_{Ca} only affected the frequency of tremor frequency activity in the intrinsic but not the extrinsic network. Reductions in S_{Ca} increased tremor frequency spectral power in the extrinsic network but led to decreases in the intrinsic network.

In the extrinsic model (Fig. 6A–F), neither reductions nor increases in S_{Ca} significantly affected the peak frequency of 6.1 Hz (Fig. 6A and Table 2). However, reductions in S_{Ca} led to significant increases in the tremor frequency band power, while

S_{Ca} increases significantly reduced the power, for all levels tested, demonstrating a strong dependence of the tremor frequency power but not the peak frequency on S_{Ca} in the extrinsic model (Fig. 6B and Table 2).

Raster data (Fig. 6C–E), as well as the spike histograms (Fig. 6F) illustrated how S_{Ca} changes affected VIM cells in the extrinsic network. With reduced S_{Ca} in the extrinsic network (Fig. 6E), the spike rasters showed stronger synchrony across the cells, as the extrinsic tremor drive had a greater contribution to the waveform width on each cycle of the oscillation. The reverse occurred with increased S_{Ca}: the T-type Ca^{2+} dynamics began to interfere with the strong extrinsic drive, leading to a partial breakdown in synchronous activity in the tremor frequency band.

In contrast to the extrinsic model, S_{Ca} changes significantly affected the peak frequency of the intrinsic network (Fig. 6G–L and Table 2), from 6.5 Hz at baseline (1.00). Both reductions tested significantly lowered the peak frequency, both staying within the tremor frequency band. In contrast, increases in S_{Ca} significantly increased the peak frequency, also staying within the tremor frequency band. These differences suggested that if blocking T-type Ca^{2+} channels altered the frequency of tremor activity in VIM, intrinsic mechanisms would be implicated, while the absence of frequency changes would be more consistent with extrinsic drive of tremor activity.

At large deviations from the baseline S_{Ca} in the intrinsic model, significant changes in power occurred. Increases in S_{Ca} led to reductions of power in the tremor band, similar to that seen in the extrinsic network. However, S_{Ca} reduction by half led to a significant decline in tremor frequency power in the intrinsic network, opposite the effect seen for the extrinsic network. This suggests that, depending on the biophysical mechanism for tremor frequency oscillations in the VIM, blocking T-type Ca^{2+} channels would have opposite effects. However, tremor frequency activity in both networks was paradoxically reduced by increases in T-type Ca^{2+}, suggesting that T-type Ca^{2+} agonists such as ST101 or SAK3 [61, 69] may work to reduce tremor in either case.

The raster data (Fig. 6I–K) and spike histograms (Fig. 6L) for the intrinsic network demonstrated different mechanisms compared to the extrinsic network. The reduction in tremor frequency activity in the intrinsic network was due to the fact that there was no external driver to support the oscillations, which were driven by the response of T-type Ca^{2+} to the phasic inhibition from TRN. Increases in S_{Ca} in the intrinsic model also partially broke down oscillatory activity, despite a simultaneous increase in the frequency (Fig. 6I).

Taken together, changes in S_{Ca} affected both extrinsic and intrinsic tremor frequency oscillations in different ways, and the model results suggested that pharmacological

manipulations of T-type Ca^{2+} activity directly in VIM lead to different outcomes. The model results predict that T-type Ca^{2+} antagonists would increase extrinsic tremor frequency activity and decrease intrinsic tremor frequency activity, while T-type Ca^{2+} agonists would reduce tremor frequency activity in either. Targeted experiments with T-type Ca^{2+} in the VIM could help to disambiguate the mechanisms underlying tremor frequency activity in VIM.

3.4 Tremor frequency power depended upon $GABA_A$ within the TRN but not from TRN to VIM

Tremor in ET is thought to involve GABA-ergic mechanisms [19, 26, 49], and medications that reduce tremor may also potentiate GABA [19]. To test the effects of site-and type-specific GABA in the models, we modulated $GABA_A$ conductances at two different sites (illustrated in Fig. 2A–B): from TRN to VIM and from TRN to TRN, shown in Fig. 7 and Table 3). We tracked the power of tremor frequency oscillations as a function of varying the conductances. Relative to baseline at 1.0, tremor power changes were calculated at GABA conductance levels of 0, 0.5, 2, and 4. While $GABA_A$ from TRN to VIM did not significantly affect tremor in either the extrinsic or intrinsic models (Fig. 7A–B), increases in TRN-TRN $GABA_A$ significantly reduced tremor power (Fig. 7C–D, Table 3).

In both networks, reductions in TRN-TRN $GABA_A$ increased tremor frequency activity relative to the respective baselines. As the conductance was increased, in both models, significant reductions in tremor frequency activity were observed. Tremor power was directly compared at each conductance level (Table 3), and the TRN-TRN $GABA_A$ conductance had a greater impact on the intrinsic versus extrinsic networks. With TRN-TRN $GABA_A$ conductance removed, the intrinsic tremor power was significantly greater than in the extrinsic network.

With increases in TRN-TRN $GABA_A$, both the extrinsic and intrinsic networks had reduced tremor frequency activity. However, the tremor frequency activity in the intrinsic network was significantly lower than that of the extrinsic network at both 2.0 and 4.0 times the baseline conductance.

In the extrinsic model, the relatively smaller changes in tremor frequency activity due to changes in TRN-TRN $GABA_A$ were due to the fact that an extrinsic drive was propagating tremor frequency activity in the network. The VIM-TRN network was more resilient to changes in these dynamics than the intrinsic network. The intrinsic network, having no external driver of tremor frequency activity, was significantly paced by the presence of internal $GABA_A$ dynamics in the TRN. When this was disturbed by increases in TRN-TRN $GABA_A$, the TRN reduced the ability for the VIM

to maintain tremor dynamics.

In both the extrinsic and intrinsic models, increased $GABA_A$ conductance within the TRN reduced tremor frequency activity in the VIM. These model results predict that precise upregulation of GABAergic activity specifically within the TRN reduce tremor.

3.5 Tremor frequency power was reduced with reductions in $GABA_B$ conductance in both models

For TRN-VIM $GABA_B$, reductions, but not increases, significantly reduced tremor frequency power (Fig. 7E–F). In the extrinsic network (Fig. 7E), the tremor power dropped at both half the conductance and with complete removal. Reductions in TRN-VIM $GABA_B$ conductance also reduced intrinsic power (Fig. 7F). Reductions in tremor power due to TRN-VIM $GABA_B$ reductions were also significantly greater for the intrinsic model compared to the extrinsic model. Extrinsic tremor frequency activity, though paced by the tremor input, was still affected by the reduction of $GABA_B$. However, intrinsic activity was strongly influenced by reductions of TRN-VIM $GABA_B$ in the model, suggesting that reducing $GABA_B$ may help to reduce tremor in certain situations.

Overall, both $GABA_A$ increases within TRN and $GABA_B$ reductions from TRN to VIM reduced tremor frequency activity in both the extrinsic and intrinsic networks. Additionally, reductions in $GABA_A$ within the TRN led to increased tremor frequency activity in the VIM, suggesting that precision in GABA modulation is important in controlling the expression of tremor.

3.6 Intrinsic tremor frequency activity was further increased by tremor periodic input

It has been suggested that tremor frequency activity may be driven by cerebellum [19, 41, 58], and it is also possible that cortex plays a role [5, 63]. Yet it is not known exactly how tremor frequency activity interacts among different regions of this circuit and specifically how extrinsic influences affect the intrinsic oscillatory capacity of the thalamus. To account for the possibility of these interactions co-occurring, we simulated intrinsic oscillations combined with a simultaneous, extrinsic 6 Hz tremor frequency input. The simulated phasic drive consisted of 30 normally distributed AMPA-ergic inputs per cycle of the 6 Hz oscillation. As the unitary input strength was increased from 1×10^{-4}–5×10^{-3} μS, tremor power was significantly increased at 5×10^{-4} and 5×10^{-3} μS (Fig. 8 and Table 4A).

These oscillations were strongly driven by the external input, which is seen in the mean fields in Fig. 8B. From baseline, as the strength of the external drive increased,

the oscillations became more regular. The increases in tremor power suggested that the intrinsic activity of the thalamus can co-exist with external influences from areas such as deep cerebellar nuclei or the primary motor cortex. Understanding the role of intrinsic and extrinsic influences on tremor frequency activity may affect tremor expression as well as therapy.

3.7 Simulated non-tremor frequency activity reduced tremor power in extrinsic network but increased tremor power in intrinsic network

Cerebellar motor and non-motor activity is transmitted from deep cerebellar nuclei to the VIM, and primary motor cortex also projects to VIM [5, 63], so we simulated how different tremor mechanisms in VIM responded to non-tremor inputs that could arise from these sources. We simulated different strengths of a Poisson-distributed AMPA-ergic input with a rate parameter λ of 25 ms (see Methods) and found that the input significantly decreased tremor power in the extrinsic model and significantly increased tremor power in the intrinsic model (Fig. 9 and Table 4B).

In the extrinsic model, as the strength of the Poisson input was increased from 2.5×10^{-5}–1×10^{-4} μS, the tremor power decreased from the baseline, significantly at 5×10^{-5} and 1×10^{-4} μS. Because the extrinsically driven tremor frequency activity was dependent upon the tremor-periodic input, an additional non-tremor input interfered, reducing the amplitude of tremor frequency activity in the network (Fig. 9Bi).

In contrast, in the intrinsic model, there was a significant increase in tremor concentration with an increase of Poisson conductance from 5.0×10^{-5}–1×10^{-4} μS. As shown in Fig. 9Bii, though the amplitude of the tremor frequency activity did not increase, the shape of the activity was more sinusoidal, due to the Poisson input promoting periods of ongoing excitation in the intrinsic tremor frequency activity.

For each Poisson input conductance tested, the resulting tremor power in the extrinsic model was directly compared to that of the intrinsic model. In each case, the tremor power was significantly less in the extrinsic model than the intrinsic model. While Poisson inputs to the extrinsic network disrupted the tremor frequency activity, they facilitated tremor frequency activity in the intrinsic network, supporting the view that non-tremor cerebellar or cortical inputs into VIM would increase tremor frequency activity if dominated by intrinsic mechanisms, while the same inputs would reduce tremor frequency activity if it is driven by extrinsic mechanisms.

4 Discussion

We simulated a network of VIM cells and TRN cells that generated tremor frequency oscillations to understand how two distinct mechanisms might contribute to the generation of tremor frequency oscillations and respond to non-tremor motor activity. "Extrinsic" tremor frequency activity was driven by tremor-periodic inputs from an external source like the dentate nucleus and the cerebellum. "Intrinsic" tremor frequency activity was generated by self-paced rhythmic activity that relied on GABA-ergic TRN inputs onto the cells in VIM and the T-type Ca^{2+} activity in both VIM and TRN cells. Both of these networks demonstrated tremor frequency field potentials consistent with those recorded in VIM during epochs of high physiological tremor, but their mechanisms of generation and responses to non-tremor activity were distinct (Fig. 4), suggesting different treatment strategies to alleviate tremor.

4.1 Origins of tremor frequency activity in VIM

The origin—or origins—of tremor frequency oscillations related to tremor in ET are not fully known. Prior work suggested that tremor frequency oscillations in the thalamus are driven by cerebellar activity [19, 41, 58], and there are multiple potential mechanisms that may all contribute to different manifestations of ET. One suggestion has been that the loss of GABA-ergic tone from Purkinje cells leads to disinhibition of the dentate nucleus and other deep cerebellar nuclei, and the intrinsic pacemaking ability of the dentate nucleus may then transmit tremor frequency activity to the thalamus. This view seems plausible considering the presence of T-type Ca^{2+} activity in deep cerebellar nuclei and limited evidence in anesthetized rodent suggesting that thalamic bursting may originate from this source [19,53].

Another hypothesis suggests that the inferior olive generates and transmits tremor frequency activity to the cerebellum and then to the thalamus [18,19,22,58]. For this to be true, the primary target of the inferior olivary nucleus, the Purkinje cells, should demonstrate tremor frequency activity, which would need to be transmitted onto the deep cerebellar nuclei [4] in order to be transmitted to the VIM. To our knowledge, direct evidence that such activity is faithfully propagated has not been fully established, but even without Purkinje cells, the effect of the inferior olivary nucleus directly on deep cerebellar nuclei needs further investigation [22]. Nevertheless, in these scenarios, the final output of the dentate nucleus would be tremor periodic, so we investigated the VIM network with the extrinsic driver as well as the impact of tremor-periodic input into the intrinsic network (Fig. 8).

A recent computational model was used to investigate various aspects of tremor in ET [70], using a mean field approach to understand network dynamics of tremor

activity, including VIM, TRN, cerebellum, and cortex. In particular, their network sustained tremor activity that was disrupted by their network model of deep brain stimulation. Here, we focused particularly on understanding how the membrane biophysics in VIM and TRN cells influenced larger-scale properties of the resulting network. To our knowledge, this is the first time the VIM-TRN network with cellular biophysics has been simulated to investigate tremor periodic activity in ET.

The pathophysiology of ET is heterogeneous [38, 41], so it is possible that certain subtypes are more consistent with extrinsic drive, while others rely more on the intrinsic oscillatory capabilities of the thalamus and other areas. Our model suggests that the actual VIM tremor frequency activity may be the consequence of both tremor-periodic drive (from any source) and the intrinsic oscillatory predisposition of the VIM. The simulations demonstrated that the mechanism by which tremor is expressed in VIM may affect the efficacy of different therapies.

4.2 Non-tremor cerebellar inputs may exacerbate tremor in VIM

The cerebellum is thought to contribute to motor planning and adaptation, and disruption of the cerebellothalamocortical pathway via lesion or deep brain stimulation (DBS) has been shown to impair these functions [13]. To understand effects of non-tremor inputs [36], we simulated Poisson-distributed synaptic inputs from cerebellum or possibly cortex that are related to features such as motor adaptation. Our results showed that non-tremor inputs potentiated intrinsic tremor and depressed extrinsic tremor (Fig. 9), suggesting that activating inputs, perhaps through a motor learning task with high cerebellar demands, would increase tremor output if intrinsic oscillations are being generated within VIM. Extrinsically paced tremor in VIM would result in a reduction in tremor during high task demands.

ET patients most typically present with an intentional tremor, in which directed movement is necessary to elicit tremor. An alternate viewpoint of the non-tremor inputs is that, when associated with movement, would exacerbate intrinsic tremor frequency mechanisms in VIM, leading to the expression of tremor only during movement. It is also possible that the movement-related activity from cerebellum gets transmitted as tremor frequency activity when any movement is made that is tremulous, but this distinction must be tested experimentally.

One candidate mechanism for the effect of DBS on reducing tremor is that targeting cerebellothalamic fibers may reduce the role of pathological cerebellar activity on the thalamus [34, 57], which is consistent with the view that tremor frequency activity is driven by cerebellar inputs. Yet the model results demonstrated that non-tremor activity also increased tremor in the intrinsic model (Fig. 9), and this increase may be

critical to the translation from tremor frequency neural activity to the expression of physiological tremor, under the assumption that tremor frequency activity in VIM drives physiological tremor rather than simply reflecting ongoing activity [50]. If tremor frequency activity in VIM must cross a threshold to drive physiological tremor expression, then DBS affecting cerebellothalamic fibers may be eliminating non-tremor inputs to VIM, still resulting in reduced tremor output despite not explicitly blocking tremor frequency input activity.

4.3 Broad effects of GABA modulation on tremor frequency activity in VIM

The implication of GABA-ergic effects ET is well established in numerous studies [1, 8, 19, 49], though many are focused on the effects of GABA in the cerebellar system and less on the direct effects of GABA in the VIM, which our results suggest may be equally important to consider.

The "GABA hypothesis" of ET suggests that disinhibition of pacemakers in the dentate nucleus may lead to increased tremor frequency activity in the thalamus and cortex [19, 49], but this remains to be demonstrated directly. In some manifestations of ET, postmortem studies have demonstrated that Purkinje cells are atrophied and degenerated, resulting in a reduction in GABA-ergic tone [42], though this is disputed [55]. Cerebellar deficiencies in ET may play a role in at least some pathology seen in ET, which may be a more heterogeneous disease than commonly thought. Ethanol, well known to reduce tremor for some patients [9], acts as a GABA agonist, and GABA is also a target for the first line pharmacological treatment of ET with propranolol and primidone [43].

In the model studied here, to generate tremor frequency oscillations in the intrinsic model, the $GABA_B$ strength was greater than that of $GABA_A$. The model results suggested that both TRN-TRN $GABA_A$ and TRN-VIM $GABA_B$ affected tremor frequency activity in the VIM-TRN circuit, while TRN-VIM $GABA_A$ did not have an effect (Fig. 7). The model result that increases in TRN-TRN $GABA_A$ reduces tremor frequency activity in VIM is consistent with observations in tremor reduction with ethanol in alcohol-responsive forms of ET.

Within the VIM, the reductions in $GABA_A$ have been implicated in tremor frequency activity, but this was not observed in the present model (Fig. 7). Microinjections of the $GABA_A$ agonist muscimol in VIM have been shown to attenuate tremor after several minutes [1]. It remains an important question how direct injections in or near TRN could affect tremor frequency activity. Under this hypothesis, similar microinjections either directly in the TRN or in more lateral or anterior to those performed previously in VIM would result in more rapid cessation of tremor,

consistent with the effects seen in the model.

There is limited evidence that the effect of muscimol may not be selective to $GABA_A$ but also affect presynaptic $GABA_B$ [66]. If true in the VIM, this would provide support for the model results. In the model, reductions in $GABA_B$—similar to the possible effects of muscimol at presynaptic sites—resulted in reduced tremor generated either by extrinsic or intrinsic mechanisms (Fig. 7E–F).

In another study using positron emission tomography, an increased binding of ^{11}C-Flumazenil at $GABA_A$ receptors was observed in the cerebellum, premotor cortex, and the VIM in ET patients compared to controls, suggesting either increased upregulation of these receptors or a deficiency in normal binding [8]. While it may be possible that this finding was in part due to deficiencies in neighboring regions of TRN, further work on $GABA_A$ and $GABA_B$ deficiencies is necessary, particularly in the VIM-TRN system.

4.4 T-type Ca^{2+} currents affected tremor frequency activity in VIM models

T-type Ca^{2+} channels have been long known to contribute to oscillatory behavior in the brain [14, 23], and they are present in areas that have been implicated in ET pathophysiology, such as the inferior olive and the dentate nucleus of the deep cerebellar nuclei. In our model of VIM, we found that changes in T-type Ca^{2+} channels affected both extrinsic and intrinsic oscillations (Fig. 6). Increased T-type Ca^{2+} conductance reduced tremor frequency activity in both extrinsic and intrinsic models, though in different ways, while significant changes in frequency were observed for intrinsic but not extrinsic oscillations. In contrast, reductions in T-type Ca^{2+} currents resulted in significant increases in extrinsic tremor frequency activity and significant decreases in intrinsic tremor frequency activity.

These channels have been also been considered as a target for ET, though primarily in the context of the olivo-cerebellar system and harmaline-induced tremor in rodents [23]. Certain T-type Ca^{2+} antagonists, such as zonisamide [37, 45], have been attempted for treatment of ET [47], but the efficacy is not yet clear [48]. Zonisamide reduces T-type Ca^{2+}, which our model suggests would lead to different effects in tremor power in VIM, depending on the prevalence of extrinsic versus intrinsic mechanisms (Fig. 6B and H). In the intrinsic model, reductions in T-type Ca^{2+} also led to a reduction in the tremor frequency (Fig. 6G).

Prior work has implicated the role of T-type Ca^{2+} channels in movement disorder pathophysiology [31, 56], suggesting that reducing or leveraging the biophysics of T-type Ca^{2+} currents, particularly as they relate to tremor frequency oscillations, may be crucial in reducing pathological tremor frequency activity from being manifested

in the VIM, with potential consequences for physiological tremor in patients. In our network, increased T-type Ca^{2+} currents reduced tremor power in both networks and also increased the frequency of intrinsic tremor oscillations (Fig. 6). Despite the role of T-type Ca^{2+} currents in promoting oscillatory activity, in both models, too much of the current desynchronized the network activity and led to paradoxically less tremor frequency activity, providing a testable experimental prediction.

In a model of coupled brainstem neurons with reciprocal inhibition that involved T-type Ca^{2+} channels, Shaikh *et al.* suggested that increased T-type Ca^{2+} currents reduced tremor frequencies and increased tremor power [59]. The differences with the present model results suggest perhaps that the specific network topology is critically important to understanding the outcomes of seemingly similar manipulations and suggests that pharmacological consequences may vary substantially depending on the anatomical site of action. Direct manipulation of T-type Ca^{2+} at relevant sites—such as the TRN, VIM, inferior olivary nucleus, and dentate nucleus—will be necessary to understand to what extent T-type Ca^{2+} disruptions at these sites can reduce tremor.

Conclusions

We recorded tremor frequency neural activity in human VIM, correlated with physiological tremor, to constrain multiple biophysical mechanisms of tremor frequency activity. We separated extrinsic and intrinsic mechanisms of tremor frequency activity in the models to study them independently. Our simulations suggested that these two distinct types of oscillations may co-exist and confer distinct properties on tremor oscillations that are important in understanding mechanisms of tremor and designing effective pharmacological or electrical treatments such as DBS. The model provides specific predictions that can be tested experimentally to understand the extent of intrinsically paced oscillations on tremor frequency activity in the thalamus and how it interacts with external influences.

Acknowledgements

This work was funded by NIMH 5T32MH019118-23, NIMH R01 MH106174 (SRJ), Brown University Dean's Emerging Areas in New Science Award (SRJ and WFA), and the Doris Duke Clinician Scientist Development Award (WFA). The authors declare no competing financial interests. We would like to thank the patients for their participation.

References

[1] Pahapill Peter A., Levy Ron, Dostrovsky Jonathan O., Davis Karen D., Rezai Ali R., Tasker Ronald R., and Lozano Andres M. Tremor arrest with thalamic microinjections of muscimol in patients with essential tremor. *Annals of Neurology*, 2001.

[2] Wael F. Asaad and Emad N. Eskandar. A flexible software tool for temporally-precise behavioral control in matlab. *Journal of Neuroscience Methods*, 2008.

[3] Wael F. Asaad, Navaneethan Santhanam, Steven McClellan, and David J. Freedman. High-performance execution of psychophysical tasks with complex visual stimuli in matlab. *Journal of Neurophysiology*, 2013.

[4] C. Asanuma, W.T. Thach, and E.G. Jones. Anatomical evidence for segregated focal groupings of efferent cells and their terminal ramifications in the cerebellothalamic pathway of the monkey. *Brain Research Reviews*, 1983.

[5] T E J Behrens, H Johansen-Berg, M W Woolrich, S M Smith, C A M Wheeler-Kingshott, P A Boulby, G J Barker, E L Sillery, K Sheehan, O Ciccarelli, A J Thompson, J M Brady, and P M Matthews. Non-invasive mapping of connections between human thalamus and cortex using diffusion imaging. *Nature Neuroscience*, 2003.

[6] Yoav Benjamini and Yosef Hochberg. Controlling the false discovery rate: A practical and powerful approach to multiple testing. 1995.

[7] Merrill J. Birdno, Wei Tang, Jonathan O. Dostrovsky, William D. Hutchison, and Warren M. Grill. Response of human thalamic neurons to high-frequency stimulation. *PLOS ONE*, 2014.

[8] Henning Boecker, Adolf Weindl, David J. Brooks, Andres O. Ceballos-Baumann, Christoph Liedtke, Matthias Miederer, Till Sprenger, Klaus J. Wagner, and Isabelle Miederer. Gabaergic dysfunction in essential tremor: An 11c-flumazenil pet study. *Journal of Nuclear Medicine*, 2010.

[9] Henning Boecker, Adrian J. Wills, Andres Ceballos-Baumann, Michael Samuel, Philip D. Thompson, Leslie J. Findley, and David J. Brooks. The effect of ethanol on alcohol-responsive essential tremor: A positron emission tomography study. *Annals of Neurology*, 1996.

[10] David T. Brocker, Brandon D. Swan, Dennis A. Turner, Robert E. Gross, Stephen B. Tatter, Mandy Miller Koop, Helen Bronte-Stewart, and Warren M. Grill. Improved

efficacy of temporally non-regular deep brain stimulation in parkinson's disease. *Experimental Neurology*, 2013.

[11] Arthur W. G. Buijink, A. M. Madelein van der Stouwe, Marja Broersma, Sarvi Sharifi, Paul F. C. Groot, Johannes D. Speelman, Natasha M. Maurits, and Anne-Fleur van Rootselaar. Motor network disruption in essential tremor: a functional and effective connectivity study. *Brain*, 2015.

[12] Nicholas T Carnevale and Michael L Hines. *The NEURON book*. Cambridge University Press, 2006.

[13] Haiyin Chen, Sherwin E. Hua, Maurice A. Smith, Frederick A. Lenz, and Reza Shadmehr. Effects of human cerebellar thalamus disruption on adaptive control of reaching. *Cerebral Cortex*, 2006.

[14] A. Destexhe, T. Bal, D. A. McCormick, and T. J. Sejnowski. Ionic mechanisms underlying synchronized oscillations and propagating waves in a model of ferret thalamic slices. *Journal of Neurophysiology*, 1996.

[15] A Destexhe, D Contreras, M Steriade, TJ Sejnowski, and JR Huguenard. In vivo, in vitro, and computational analysis of dendritic calcium currents in thalamic reticular neurons. *The Journal of Neuroscience*, 1996.

[16] Alain Destexhe, Mike Neubig, Daniel Ulrich, and John Huguenard. Dendritic low-threshold calcium currents in thalamic relay cells. *The Journal of Neuroscience*, 1998.

[17] G. Deuschl, R. Wenzelburger, K. Löffler, J. Raethjen, and H. Stolze. Essential tremor and cerebellar dysfunction clinical and kinematic analysis of intention tremor. *Brain*, 2000.

[18] Günther Deuschl and Hagai Bergman. Pathophysiology of nonparkinsonian tremors. *Movement Disorders*, 2002.

[19] Alexandre Gironell. The gaba hypothesis in essential tremor: lights and shadows. *Tremor and other hyperkinetic movements*, 2014.

[20] Robert E. Gross, Edward G. Jones, Jonathan O. Dostrovsky, Catherine Bergeron, Anthony E. Lang, and Andres M. Lozano. Histological analysis of the location of effective thalamic stimulation for tremor. *Journal of Neurosurgery*, 2004.

[21] Mark Hallett. Tremor: Pathophysiology. *Parkinsonism & Related Disorders*, 2014.

[22] Adrian Handforth. Harmaline tremor: underlying mechanisms in a potential animal model of essential tremor. *Tremor and Other Hyperkinetic Movements*, 2012.

[23] Adrian Handforth, Gregg E. Homanics, Douglas F. Covey, Kathiresan Krishnan, Jae Yeol Lee, Kenji Sakimura, Fredricka C. Martin, and Arnulfo Quesada. T-type calcium channel antagonists suppress tremor in two mouse models of essential tremor. *Neuropharmacology*, 2010.

[24] B Hellwig, S Häußler, B Schelter, M Lauk, B Guschlbauer, J Timmer, and CH Lücking. Tremor-correlated cortical activity in essential tremor. *The Lancet*, 2001.

[25] B Hellwig, B Schelter, B Guschlbauer, J Timmer, and CH Lücking. Dynamic synchronisation of central oscillators in essential tremor. *Clinical Neurophysiology*, 2003.

[26] Rick C. Helmich, Ivan Toni, Günther Deuschl, and Bastiaan R. Bloem. The pathophysiology of essential tremor and parkinson's tremor. *Current Neurology and Neuroscience Reports*, 2013.

[27] Michael Hines, Andrew Davison, and Eilif Muller. Neuron and python. *Frontiers in Neuroinformatics*, 2009.

[28] T Hirai, Y Nagaseki, H Wada, T Shibazaki, M Matsumura, and C Ohye. Cell sparse zones in the ventrolateral thalamic mass in humans, monkeys and cats: their special reference to kinesthetic neurons. *Stereotactic and Functional Neurosurgery*, 1985.

[29] S E Hua, F A Lenz, T A Zirh, S G Reich, and P M Dougherty. Thalamic neuronal activity correlated with essential tremor. *Journal of Neurology, Neurosurgery & Psychiatry*, 1998.

[30] Sherwin E. Hua and Frederick A. Lenz. Posture-related oscillations in human cerebellar thalamus in essential tremor are enabled by voluntary motor circuits. *Journal of Neurophysiology*, 2004.

[31] D. Jeanmonod, M. Magnin, and A. Morel. Low-threshold calcium spike bursts in the human thalamus. common physiopathology for sensory, motor and limbic positive symptoms. *Brain*, 1996.

[32] Stephanie R. Jones, Dominique L. Pritchett, Michael A. Sikora, Steven M. Stufflebeam, Matti Hämäläinen, and Christopher I. Moore. Quantitative Analysis and Biophysically Realistic Neural Modeling of the MEG Mu Rhythm: Rhythmogenesis and Modulation of Sensory-Evoked Responses. *Journal of Neurophysiology*, 2009.

[33] Abdoul Kane, William D. Hutchison, Mojgan Hodaie, Andres M. Lozano, and Jonathan O. Dostrovsky. Enhanced synchronization of thalamic theta band local field potentials in patients with essential tremor. *Experimental Neurology*, 2009.

[34] Maureen Keane, Steve Deyo, Aviva Abosch, Jawad A Bajwa, and Matthew D Johnson. Improved spatial targeting with directionally segmented deep brain stimulation leads for treating. *Journal of Neural Engineering*, 2012.

[35] Seon-Min Lee, Minjik Kim, Hye Mi Lee, Kyum-Yil Kwon, and Seong-Beom Koh. Nonmotor symptoms in essential tremor: Comparison with parkinson's disease and normal control. *Journal of the Neurological Sciences*, 2015.

[36] Shane Lee, Wael F. Asaad, and Stephanie R. Jones. Computational modeling to improve treatments for essential tremor. *Drug Discovery Today: Disease Models*, 2017.

[37] Ilo E. Leppik. Zonisamide: chemistry, mechanism of action, and pharmacokinetics. *Seizure*, 2004.

[38] Elan D. Louis. Essential tremor. *The Lancet Neurology*, 2005.

[39] Elan D. Louis and Joaquim J. Ferreira. How common is the most common adult movement disorder? update on the worldwide prevalence of essential tremor. *Movement Disorders*, 2010.

[40] Elan D. Louis, Ruth Ottman, and W. Allen Hauser. How common is the most common adult movement disorder? estimates of the prevalence of essential tremor throughout the world. *Movement Disorders*, 1998.

[41] Elan D. Louis and Jean Paul G. Vonsattel. The emerging neuropathology of essential tremor. *Movement Disorders*, 2008.

[42] Elan D. Louis, Hong Yi, Cordelia Erickson-Davis, Jean-Paul G. Vonsattel, and Phyllis L. Faust. Structural study of purkinje cell axonal torpedoes in essential tremor. *Neuroscience Letters*, 2009.

[43] Judit Mally and Trevor W. Stone. The effect of theophylline on essential tremor: The possible role of gaba. *Pharmacology Biochemistry and Behavior*, 1991.

[44] H. B. Mann and D. R. Whitney. On a test of whether one of two random variables is stochastically larger than the other. *Ann. Math. Statist.*, 1947.

[45] Nora Matar, Wei Jin, Heiko Wrubel, Jürgen Hescheler, Toni Schneider, and Marco Weiergräber. Zonisamide block of cloned human t-type voltage-gated calcium channels. *Epilepsy Research*, 2009.

[46] Cameron C. McIntyre, Warren M. Grill, David L. Sherman, and Nitish V. Thakor. Cellular effects of deep brain stimulation: Model-based analysis of activation and inhibition. *Journal of Neurophysiology*, 2004.

[47] Shuhei Morita, Hideto Miwa, and Tomoyoshi Kondo. Effect of zonisamide on essential tremor: a pilot crossover study in comparison with arotinolol. *Parkinsonism & Related Disorders*, 2005.

[48] William G. Ondo. Zonisamide for essential tremor. *Clinical Neuropharmacology*, 2007.

[49] Sarah Paris-Robidas, Elodie Brochu, Marion Sintes, Vincent Emond, Mélanie Bousquet, Milène Vandal, Mireille Pilote, Cyntia Tremblay, Thérèse Di Paolo, Ali H. Rajput, Alex Rajput, and Frédéric Calon. Defective dentate nucleus gaba receptors in essential tremor. *Brain*, 2012.

[50] David J. Pedrosa, Eva-Lotte Quatuor, Christiane Reck, K. Amande M. Pauls, Carlo A. Huber, Veerle Visser-Vandewalle, and Lars Timmermann. Thalamomuscular coherence in essential tremor: Hen or egg in the emergence of tremor? *The Journal of Neuroscience*, 2014.

[51] David J. Pedrosa, Christiane Reck, Esther Florin, K. Amande M. Pauls, Mohammad Maarouf, Lars Wojtecki, Haidar Salimi Dafsari, Volker Sturm, Alfons Schnitzler, Gereon R. Fink, and Lars Timmermann. Essential tremor and tremor in parkinson's disease are associated with distinct 'tremor clusters' in the ventral thalamus. *Experimental Neurology*, 2012.

[52] Didier Pinault. The thalamic reticular nucleus: structure, function and concept. *Brain Research Reviews*, 2004.

[53] Didier Pinault and Martin Deschênes. The origin of rhythmic fast subthreshold depolarizations in thalamic relay cells of rats under urethane anaesthesia. *Brain Research*, 1992.

[54] Jan Raethjen and Günther Deuschl. The oscillating central network of essential tremor. *Clinical Neurophysiology*, 2012.

[55] A.H. Rajput, C.A. Robinson, M.L. Rajput, S.L. Robinson, and A. Rajput. Essential tremor is not dependent upon cerebellar purkinje cell loss. *Parkinsonism & Related Disorders*, 2012.

[56] Jonathan E. Rubin and David Terman. High frequency stimulation of the subthalamic nucleus eliminates pathological thalamic rhythmicity in a computational model. *Journal of Computational Neuroscience*, 2004.

[57] Ulrika Sandvik, Lars-Owe Koskinen, Anders Lundquist, and Patric Blomstedt. Thalamic and subthalamic deep brain stimulation for essential tremorwhere is the optimal target? *Neurosurgery*, 2012.

[58] Alfons Schnitzler, Christian Münks, Markus Butz, Lars Timmermann, and Joachim Gross. Synchronized brain network associated with essential tremor as revealed by magnetoencephalography. *Movement Disorders*, 2009.

[59] Aasef G. Shaikh, Kenichiro Miura, Lance M. Optican, Stefano Ramat, Robert M. Tripp, and David S. Zee. Hypothetical membrane mechanisms in essential tremor. *Journal of Translational Medicine*, 2008.

[60] S.Murray Sherman. Tonic and burst firing: dual modes of thalamocortical relay. *Trends in Neurosciences*, 2001.

[61] Moriguchi Shigeki, Shioda Norifumi, Yamamoto Yui, Tagashira Hideaki, and Fukunaga Kohji. The T-type voltage-gated calcium channel as a molecular target of the novel cognitive enhancer ST101: enhancement of long-term potentiation and CaMKII autophosphorylation in rat cortical slices. *Journal of Neurochemistry*, 2012.

[62] Carlos Singer, Juan Sanchez-Ramos, and William J. Weiner. Gait abnormality in essential tremor. *Movement Disorders*, 1994.

[63] Iwona Stepniewska, Todd M. Preuss, and Jon H. Kaas. Thalamic connections of the primary motor cortex (M1) of owl monkeys. *The Journal of Comparative Neurology*, 1994.

[64] Henning Stolze, Gesche Petersen, Jan Raethjen, Roland Wenzelburger, and Günther Deuschl. The gait disorder of advanced essential tremor. *Brain*, 2001.

[65] Brandon D. Swan, David T. Brocker, Justin D. Hilliard, Stephen B. Tatter, Robert E. Gross, Dennis A. Turner, and Warren M. Grill. Short pauses in thalamic deep brain stimulation promote tremor and neuronal bursting. *Clinical Neurophysiology*, 2016.

[66] Yamauchi Tatsuhito, Hori Tetsuya, and Takahashi Tomoyuki. Presynaptic inhibition by muscimol through gabab receptors. *European Journal of Neuroscience*, 2001.

[67] W T Thach. Discharge of cerebellar neurons related to two maintained postures and two prompt movements. i. nuclear cell output. *Journal of Neurophysiology*, 1970.

[68] Frank Wilcoxon. Individual comparisons by ranking methods. *Biometrics bulletin*, 1945.

[69] Yasushi Yabuki, Kazuya Matsuo, Hisanao Izumi, Hidaka Haga, Takashi Yoshida, Minoru Wakamori, Akikazu Kakei, Kenji Sakimura, Takaichi Fukuda, and Kohji Fukunaga. Pharmacological properties of SAK3, a novel T-type voltage-gated Ca2+ channel enhancer. *Neuropharmacology*, 2017.

[70] Nada Yousif, Michael Mace, Nicola Pavese, Roman Borisyuk, Dipankar Nandi, and Peter Bain. A network model of local field potential activity in essential tremor and the impact of deep brain stimulation. *PLOS Computational Biology*, 2017.

Tables

Table 1: **Key parameters compared to original model.** Original model shaded in gray. A. Compartments in each section of the cells in the model. B. Geometry and biophysics from original model of thalamocortical cells [16] and the present VIM cell. C. Geometry and biophysics from the original model of TRN cells [14] and the present TRN cell.

A	Original Model Thalamocortical Cell	VIM Cell	Original Model TRN Cell	TRN Cell
Somatic Compartments	1	1	1	1
Dendritic Compartments	2	6	2	4
Axonal Compartments	—	1	—	1

B	Original Model Thalamocortical Cell Soma	VIM Cell Soma	Original Model Thalamocortical Cell Proximal Dendrite	VIM Cell Proximal Dendrites	Original Model Thalamocortical Cell Distal Dendrite	VIM Cell Distal Dendrites	VIM Cell Axon
L (μm)	38.42	16.92	12.49	12.49	84.67	84.67	2500
d (μm)	26.00	16.92	10.28	10.28	8.50	8.50	2.00
C (μF/cm^2)	7.00	4.25	8.83	4.25	8.83	4.25	0.10
ρ (Ω cm)	173	173	173	173	173	173	70.0
g_{Na} (S/cm^2)	0.10	0.90	—	—	—	—	0.21
E_{Na} (mV)	50.0	50.0	—	—	—	—	40.0
V_{shift}	-52.0	-52.0	—	—	—	—	-50.0
g_K (S/cm^2)	0.10	0.30	—	—	—	—	0.20
E_K (mV)	-100.00	-100.00	—	—	—	—	-80.00
g_{KL} (S/cm^2)	—	$4x10^{-5}$	—	$4x10^{-5}$	—	$4x10^{-5}$	—
E_{KL} (mV)	—	-100.0	—	-100.0	—	-100.0	—
g_L (S/cm^2)	$1.00x10^{-6}$	$1.61x10^{-4}$	$3.01x10^{-4}$	$3.01x10^{-4}$	$3.01x10^{-4}$	$3.01x10^{-4}$	$1.00x10^{-6}$
E_L (mV)	-76.5	-76.5	-76.5	-76.5	-76.5	-76.5	-76.5
ρ_{TCa} (cm/s)	$1.75x10^{-5}$	$1.75x10^{-5}$	$7.56x10^{-4}$	$4.04x10^{-4}$	$7.56x10^{-4}$	$4.04x10^{-5}$	—
S_{Ca}	1.0	5.1	1.0	5.1	1.0	5.1	—
depth (μm)	0.795	0.425	0.795	0.425	0.795	0.425	—

C	Original Model TRN Cell Soma	TRN Cell Soma	Original Model TRN Cell Proximal Dendrite	TRN Cell Proximal Dendrites	Original Model TRN Cell Distal Dendrite	TRN Cell Distal Dendrites	TRN Cell Axon
L (μm)	34.5460	14.0754	103.24	103.24	190.69	190.69	2800
d (μm)	14.0754	14.0754	5.56	5.56	3.06	3.06	2.00
C (μF/cm^2)	1.000	1.000	3.777	2.750	3.777	2.750	0.10
ρ (Ω cm)	260	260	260	260	260	260	170.0
g_{Na} (S/cm^2)	0.10	0.15	—	—	—	—	0.03
E_{Na} (mV)	50.0	50.0	—	—	—	—	40.0
V_{shift}	-67.0	-67.0	—	—	—	—	-50.0
g_K (S/cm^2)	0.08	0.08	—	—	—	—	0.05
E_K (mV)	-100.0	-100.0	—	—	—	—	-80.0
g_L (S/cm^2)	$5.00x10^{-5}$	$3.00x10^{-5}$	$1.89x10^{-4}$	$1.00x10^{-4}$	$1.89x10^{-4}$	$1.00x10^{-4}$	$1.50x10^{-4}$
E_L (mV)	48.5	50.0	-82.0	-87.0	-82.0	-87.0	-67.0
g_{TCa} (S/cm^2)	$4.50x10^{-5}$	$3.00x10^{-5}$	$1.70x10^{-4}$	$4.50x10^{-5}$	$2.57x10^{-3}$	$6.50x10^{-4}$	—
S_{Ca}	1.0	1.5	1.0	1.5	1.0	1.5	—
depth (μm)	3.777	2.750	3.777	2.750	3.777	2.750	—

Table 2: **Modulation of tremor frequency activity by T-type Ca^{2+} Conductance in models.**

A. Extrinsic Model

Relative T-Type Ca^{2+} Conductance	0.50	0.75	1.0 (S_{Ca} = 5.1)	1.25	1.50	1.75	2.00
Peak Frequency (Hz)	6.10±0.00 p=0.500	6.10±0.00 p=0.500	6.10±0.00	6.10±0.00 p=0.500	6.10±0.00 p=0.500	6.10±0.00 p=0.500	6.65±0.55 p=0.184
Tremor Frequency Power	* 1.098±0.036 p=3.8x10^{-4}	* 1.063±0.038 p=0.004	1.000±0.051 (0.573±0.029 mV^2/Hz)	* 0.921±0.056 p=0.023	* 0.845±0.078 p=2.91x10^{-4}	* 0.704±0.137 p=9.13x10^{-5}	* 0.627±0.165 p=9.13x10^{-5}

B. Intrinsic Model

Relative T-Type Ca^{2+} Conductance	0.50	0.75	1.0 (S_{Ca} = 5.1)	1.25	1.50	1.75	2.00
Peak Frequency (Hz)	* 5.49±0.00 p=2.55x10^{-5}	* 6.10±0.00 p=7.14x10^{-3}	6.53±0.18	6.59±0.15 p=0.326	6.59±0.15 p=0.326	6.90±0.18 p=0.046	* 7.51±0.24 p=0.002
Tremor Frequency Power	* 0.945±0.079 p=0.013	1.045±0.047 p=0.425	1.000±0.172 (0.575±0.033 mV^2/Hz)	1.034±0.078 p=0.455	1.002±0.105 p=0.339	* 0.877±0.157 p=0.023	* 0.782±0.226 p=0.006

Table 3: **Modulation of tremor frequency power by GABA Conductance in models.**

A. $GABA_A$ TRN-VIM

Relative Conductance	0.0	0.5	1.0 ($2.5x10^{-5}$ mS/cm^2)	2.0	4.0
***Extrinsic* Relative Tremor Spectral Power**	1.026±0.009 p=0.137	0.982±0.010 p=0.260	1.000±0.007 (0.577 mV^2/Hz)	1.005±0.006 p=0.367	0.994±0.008 p=0.339
***Intrinsic* Relative Tremor Spectral Power**	0.989±0.008 p=0.339	0.993±0.006 p=0.312	1.000±0.012 (0.597 mV^2/Hz)	0.977±0.015 p=0.312	0.985±0.013 p=0.367
Comparison of Extrinsic and Intrinsic	p=0.485	p=0.038	p=0.081	p=0.192	p=0.093

B. $GABA_A$ TRN-TRN

Relative Conductance	0.0	0.5	1.0 ($5x10^{-4}$ mS/cm^2)	2.0	4.0
***Extrinsic* Relative Tremor Spectral Power**	* 1.073±0.007 p=0.007	* 1.076±0.007 p=0.005	1.000±0.010 (0.572 mV^2/Hz)	* 0.956±0.006 p=0.023	* 0.939±0.011 p=0.023
***Intrinsic* Relative Tremor Spectral Power**	* 1.117±0.012 p=$8.53x10^{-4}$	1.048±0.005 p=0.027	1.000±0.011 (0.586 mV^2/Hz)	* 0.707±0.023 p=$1.23x10^{-4}$	* 0.476±0.015 p=$9.13x10^{-5}$
Comparison of Extrinsic and Intrinsic	* p=0.006	p=0.485	p=0.192	* p=$2.20x10^{-4}$	* p=$9.13x10^{-5}$

C. $GABA_B$ TRN-VIM

Relative Conductance	0.0	0.5	1.0 ($1.5x10^{-4}$ mS/cm^2)	2.0	4.0
***Extrinsic* Relative Tremor Spectral Power**	* 0.956±0.006 p=0.006	* 0.880±0.010 p=$5.04x10^{-4}$	1.000±0.007 (0.594 mV^2/Hz)	0.996±0.007 p=0.312	0.976±0.010 p=0.192
***Intrinsic* Relative Tremor Spectral Power**	* 0.476±0.014 p=$9.13x10^{-5}$	* 0.493±0.017 p=$9.13x10^{-5}$	1.000±0.014 (0.575 mV^2/Hz)	1.019±0.010 p=0.339	1.003±0.014 p=0.455
Comparison of Extrinsic and Intrinsic	* p=$9.13x10^{-5}$	* p=$9.13x10^{-5}$	p=0.214	p=0.396	p=0.455

Table 4: **Modulation of tremor frequency power by synaptic inputs in models.** A. Tremor-periodic inputs into the intrinsic network increased tremor. B. Non-tremor inputs increased tremor in intrinsic network but not extrinsic network.

A. Tremor-periodic Input into Intrinsic Network

Unitary Input Strength (μS)	0.00	$1x10^{-4}$	$5x10^{-4}$	$1x10^{-3}$	$5x10^{-2}$
Tremor Frequency Power	1.000±0.109 (0.601±0.007 mV^2/Hz)	1.000±0.010 p=0.425	* 1.033±0.009 p=0.023	1.028±0.010 p=0.027	* 1.045±0.008 p=0.001

B. Poisson-distributed Input

Unitary Input Strength (μS)	0.00	$2.5x10^{-5}$	$5.0x10^{-5}$	$7.5x10^{-5}$	$1.0x10^{-4}$
***Extrinsic* Tremor Frequency Power**	1.000±0.012 (0.586±0.007 mV^2/Hz)	0.975±0.018 0.136	* 0.948±0.014 p=0.016	0.967±0.017 p=0.052	* 0.906±0.015 $p=5.04x10^{-4}$
***Intrinsic* Tremor Frequency Power**	1.000±0.011 (0.589±0.011 mV^2/Hz)	1.035±0.008 p=0.084	* 1.056±0.013 p=0.015	* 1.052±0.014 p=0.024	1.027±0.015 p=0.132
Comparison of Extrinsic and Intrinsic	p=0.299	* $p=2.17x10^{-3}$	* $p=1.88x10^{-4}$	* $p=1.10x10^{-3}$	* $p=1.88x10^{-4}$

Figures

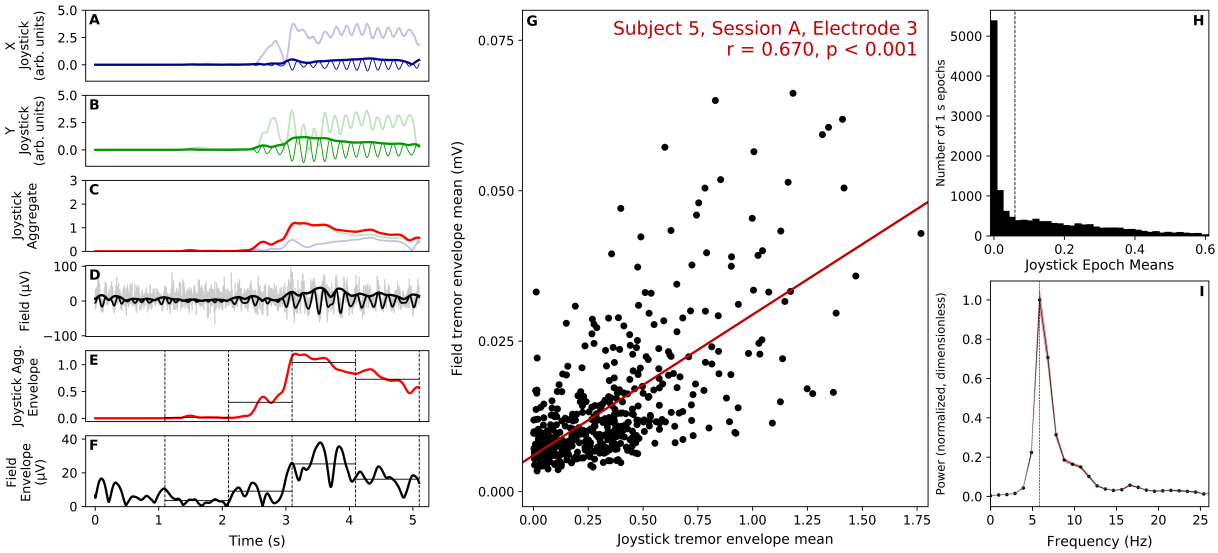

Figure 1: **Significant VIM tremor frequency activity during physiological tremor.** Thirty-one out of 44 microelectrode locations in 5 subjects showed significant linear correlation of the tremor frequency field amplitude to the physiological tremor during a center-out joystick task. Peak frequency of VIM fields was 5.9 Hz. Shown is the method used to identify recording sites with significant tremor frequency activity in VIM. A–B. X and Y components of cursor (arb. units) controlled by joystick were isolated and filtered at tremor frequencies (4–10 Hz). Envelopes (dark lines) were calculated with the Hilbert transform. C. Euclidean composite of the X and Y envelopes (red). D. Raw local field potential (gray) was tremor frequency filtered (black), and the envelope was also calculated (black). E–F. Means of joystick aggregate envelope and field envelope were calculated in 1 s epochs. G. Example electrode with Pearson correlation coefficient between joystick tremor and field tremor calculated. Red line is linear fit of these data. P values for sessions were then Benjamini-Hochberg corrected. H. From electrodes with significant tremor-correlated activity with joystick, mean physiological tremor magnitudes of non-overlapping 1 s epochs (n=14,108). Dotted line denotes median of 0.0596 (arb. units). Field activity corresponding to top half of physiological tremor was examined. I. Power spectra from the top half of significantly correlated fields (n=7054 spectra) were averaged and normalized to the spectrum peak. Red region denotes standard error.

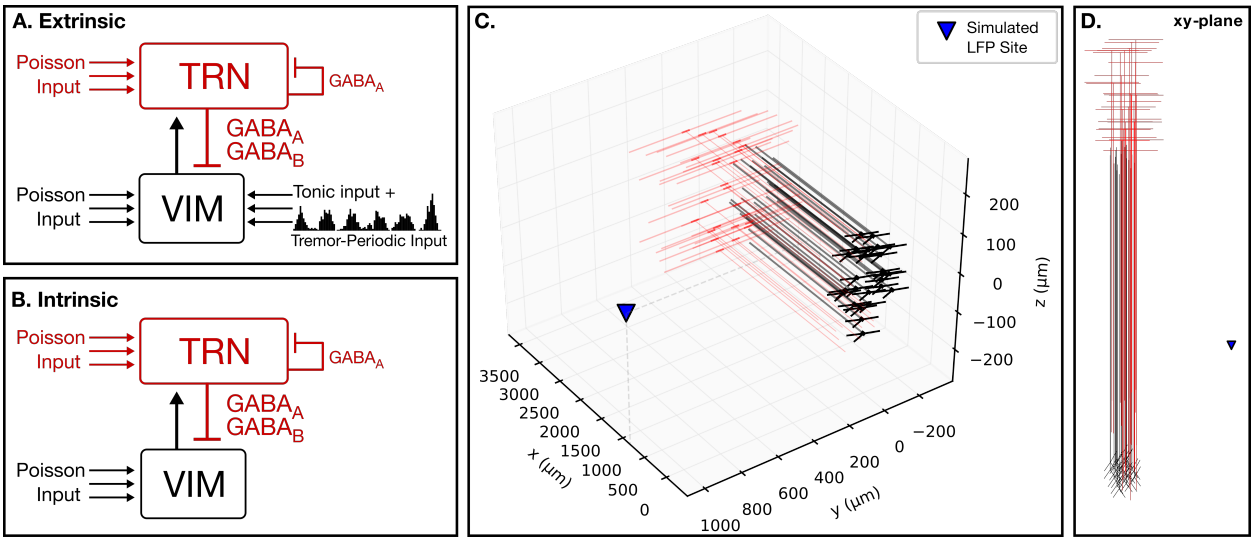

Figure 2: **Model VIM-TRN networks.** 25 multicompartment VIM cells (black) and 25 multicompartment TRN cells (red) were simulated. Background Poisson-distributed input was delivered to all cells. A. The "extrinsic" network generated tremor frequency oscillations through a combination of a phasic, tremor frequency synaptic input and tonic applied current input to the VIM cells. VIM cells made AMPA-ergic synaptic connections with the TRN cells, and TRN cells made GABA-ergic connections back to the VIM and also $GABA_A$ connections within the TRN cells. B. The "intrinsic" network generated tremor frequency oscillations that were a product of glutamatergic excitation of TRN cells and reciprocal GABA-ergic inhibition of VIM cells, which caused post-inhibition rebound. This network was initiated by only the Poisson input to the VIM and TRN cells (see Methods). C. 3D perspective of network. Extracellular recording was simulated about at (1250, 1000, 0) μm (blue triangle). D. xy-plane perspective. The center of mass of the VIM centered about the origin (0, 0, 0), with axons in the positive x direction toward the TRN. Both VIM and TRN cells in the networks received Poisson input.

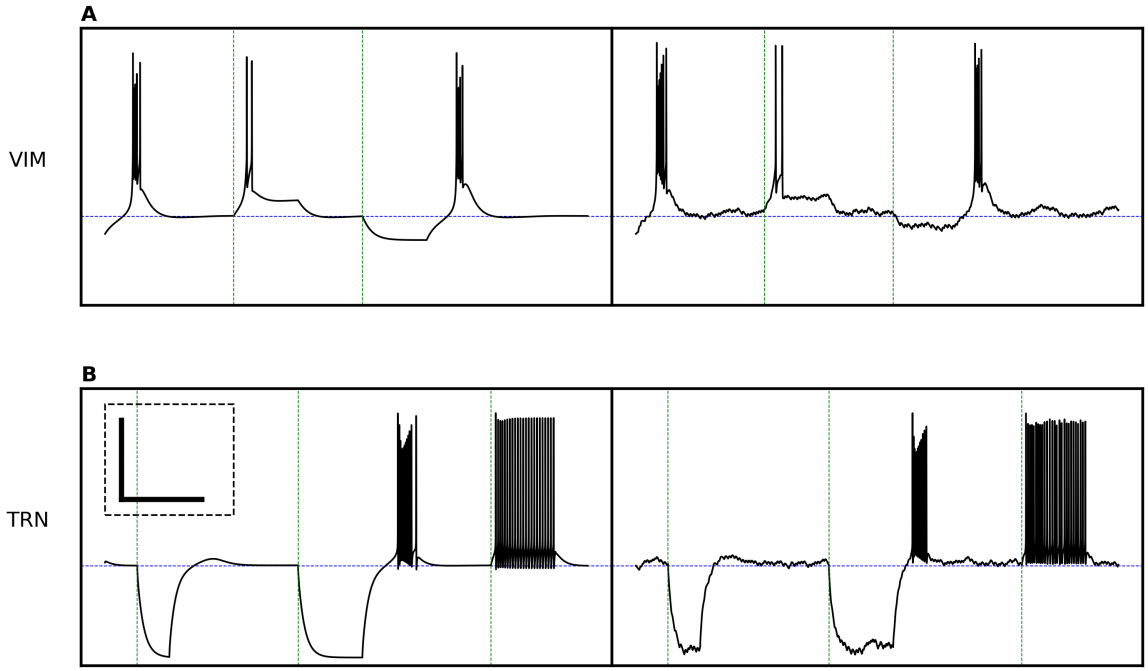

Figure 3: **Model cells replicate original models.** The VIM (A) and TRN (B) cells were modeled after Destexhe et al 1996 and 1998 [15, 16]. The original cells consisted of 3 compartments; here the VIM cells are 8 compartments (soma, 6 dendritic compartments, and an axon), and the TRN cells are 6 compartments (soma, 4 dendritic compartments, and an axon); see text for further details. For both cell types, 1.5 s are shown, the original cells are on the left, and the cells in the present model are on the right. Poisson-distributed synaptic noise was applied to the new cells. A. For the VIM cells, the horizontal line is drawn at -74 mV. Both the original and the new cells were initiated at -80 mV, eliciting a burst of spikes. At 0.4 s (first green line), positive current was injected in the VIM cells for 0.2 s, giving rise to a doublet of spikes in each case. Finally, an inhibiting current was injected at 0.8 s for 0.2 s, and upon release, both VIM cells showed similar rebound spiking before returning to baseline. B. For the TRN cells, the blue line marks -67 mV, the voltage at which the cells were initiated. At 0.1 s, for 0.1 s, a negative current was applied to the TRN cells, and no rebound spiking followed. However, at 0.6 s, the same negative amplitude current was applied for 0.2 s and elicited burst spiking in each of the cells. At 1.2 s, a positive current pulse of 0.2 s led to tonic spiking in both cells. Inset in original TRN cells applies to all plots; x scale is 0.25 s, and y scale is 50 mV.

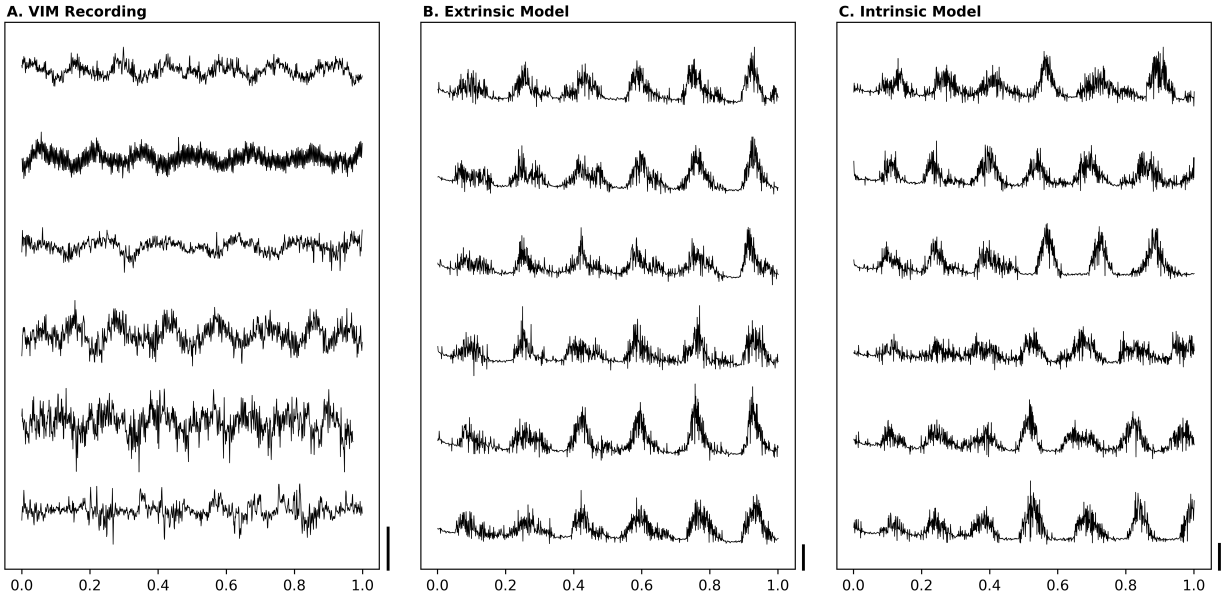

Figure 4: **Field examples of recorded tremor frequency oscillations in VIM data and in model.** Tremor frequency field activity observed in VIM (see Fig. 1). A. Six example traces of tremor frequency field oscillations recorded in VIM. Scale bar for data is 100 μV. B. Six example traces of extrinsic tremor frequency oscillations in the reduced model of 50 cells. C. Six example traces of intrinsic oscillations in the reduced model. Scale bars for B–C are 0.200 μV. Time for A–C is in seconds.

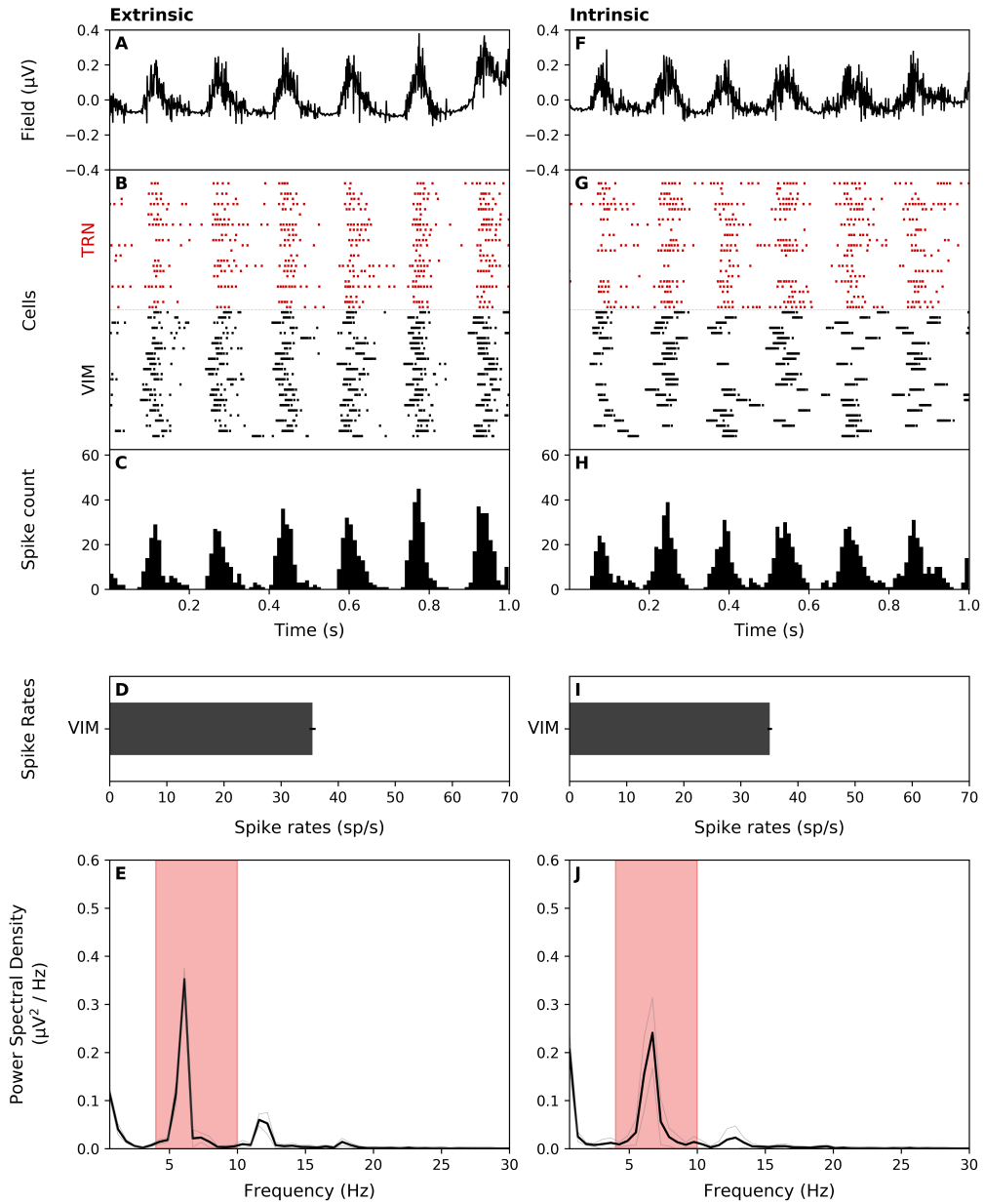

Figure 5: **Extrinsic and intrinsic models of tremor frequency oscillations showed similar properties.** A–E. Extrinsic tremor frequency oscillations were generated from tremor periodic synaptic drive. Data shown are simulated extracellular field (A), cell spike rasters for VIM (black) and TRN (red) cells (B), spike count histogram for VIM cells (C), mean VIM cell spike rates for all simulations (D), and mean power spectrum of spike count convolution for all simulations, with tremor spectral region highlighted in red (E). F–J. Same data for intrinsic oscillations that relied on VIM-TRN interactions. Mean VIM spike rates and tremor spectral concentration were not significantly different in these models. Spectral power at tremor frequencies (4–10 Hz) were also not significantly different.

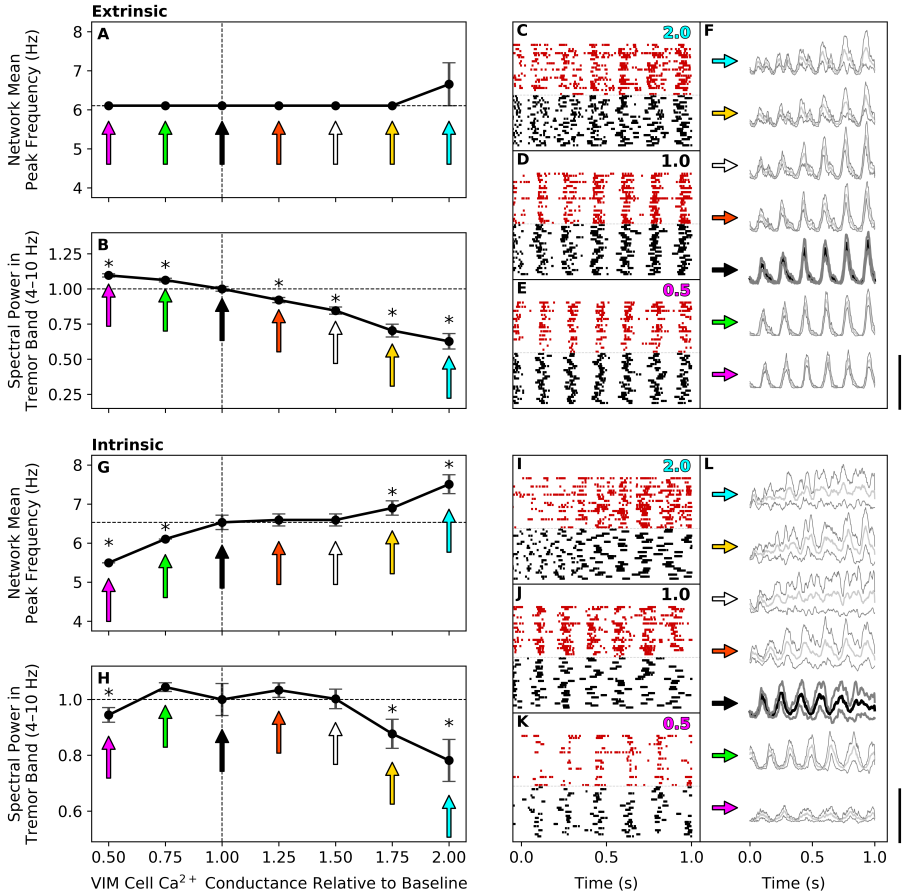

Figure 6: **Changes in T-type Ca^{2+} conductance affect both extrinsic and intrinsic tremor frequency activity.** T-type Ca^{2+} conductance changes changed spectral power in both networks but affected frequency only for the intrinsic network. S_{Ca} at baseline (1.0) was 5.1 (see Methods), and changes affected all T-type Ca^{2+} conductances in VIM cells but not TRN cells. Scale bar for F and L is 25 sp/s. All comparisons to baseline at 1.00. Values in Table 2. A–F. Extrinsic model. A. Changes in S_{Ca} did not affect the peak frequency significantly. B. Reductions in S_{Ca} increased tremor frequency activity, as the extrinsic input was the sole, rhythmic driver to the network. S_{Ca} increases reduced tremor frequency activity, as the temporal dynamics of T-type Ca^{2+} were strained. C–E. VIM (black) and TRN (red) spike rasters for examples at 2.0 (C), 1.0 (D), and 0.5 (E). F. Averaged spike convolutions with standard error for each conductance level; colors correspond to A and B. G–K. Intrinsic model. G. Increases in S_{Ca} increased the peak frequency but still within the tremor frequency range, and S_{Ca} decreases reduced the peak frequency. T-type Ca^{2+} dynamics influenced the properties of tremor activity in the absence of an external periodic driver. H. Increases in S_{Ca} reduced power in the tremor frequency band, as in the extrinsic network, but in contrast, decreases also led to a significant reduction. In the absence of an external driver, the intrinsic model required T-type Ca^{2+} dynamics to sustain the strength of tremor frequency activity. I–K. VIM (black) and TRN (red) spike rasters for examples at 2.0 (I), 1.0 (J), and 0.5 (K). L. Averaged spike convolutions with standard error for each conductance level; colors correspond to G and H.

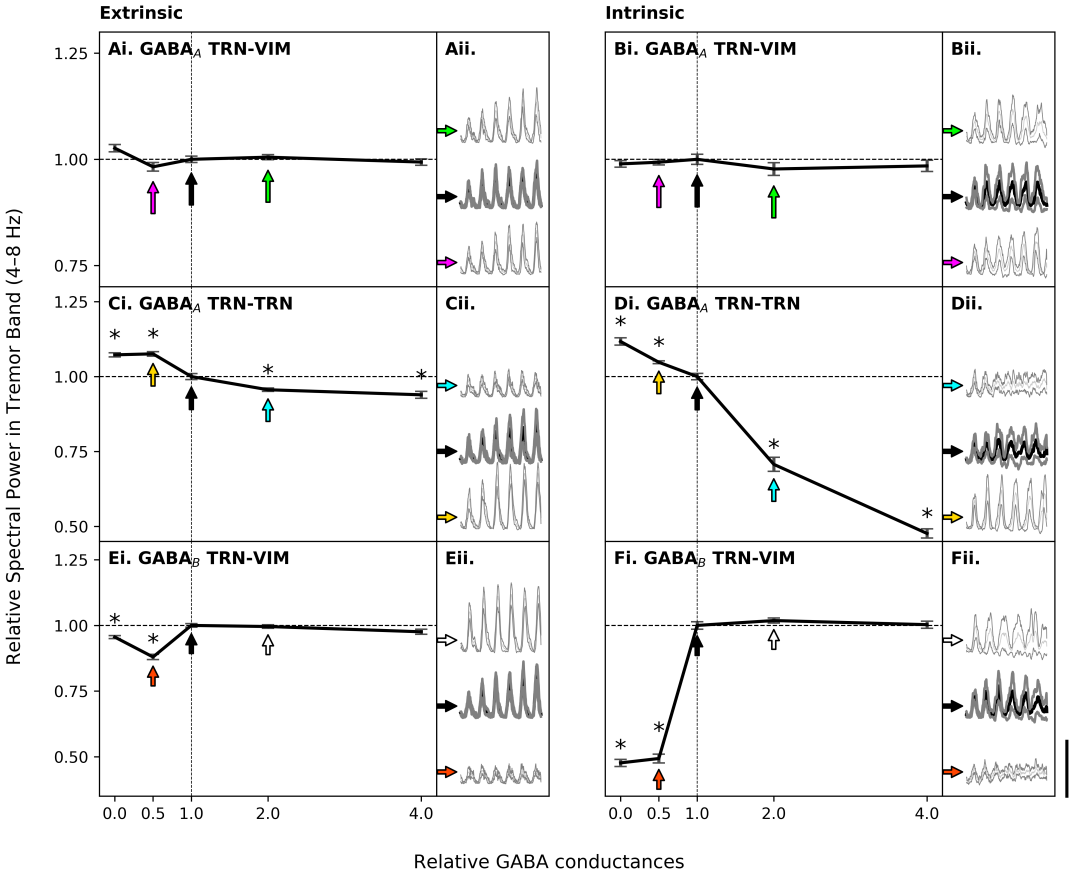

Figure 7: **Tremor frequency power varied by GABA type in both models.** Conductances of TRN-VIM $GABA_A$, TRN-TRN $GABA_A$, and TRN-VIM $GABA_B$ were varied from baseline (normalized 1.0). Differences in tremor frequency power from baseline are plotted as a function of relative conductance. Colored arrows in i panels correspond to mean spike histograms in ii panels. Scale bar for all spike histograms is 25 sp/s. Values in Table 3. A–B. $GABA_A$ from TRN-VIM. No changes affected tremor frequency power for either the extrinsic or intrinsic models. C–D. $GABA_A$ from TRN-TRN. For both extrinsic and intrinsic networks, increases in conductance reduced tremor frequency power, and reductions in conductance increased tremor frequency power, suggesting that a global increase in $GABA_A$-ergic tone may reduce tremor by affecting TRN-TRN. Total removal led to significantly greater increases in tremor activity in the intrinsic compared to the extrinsic network. Increases at 2.0 and 4.0 led to significantly lower tremor in the intrinsic compared to the extrinsic network. E–F. $GABA_B$ from TRN-VIM. For both extrinsic and intrinsic networks, reductions in conductance reduced tremor frequency power, and tremor frequency power values in the intrinsic network were significantly lower than in the extrinsic network.

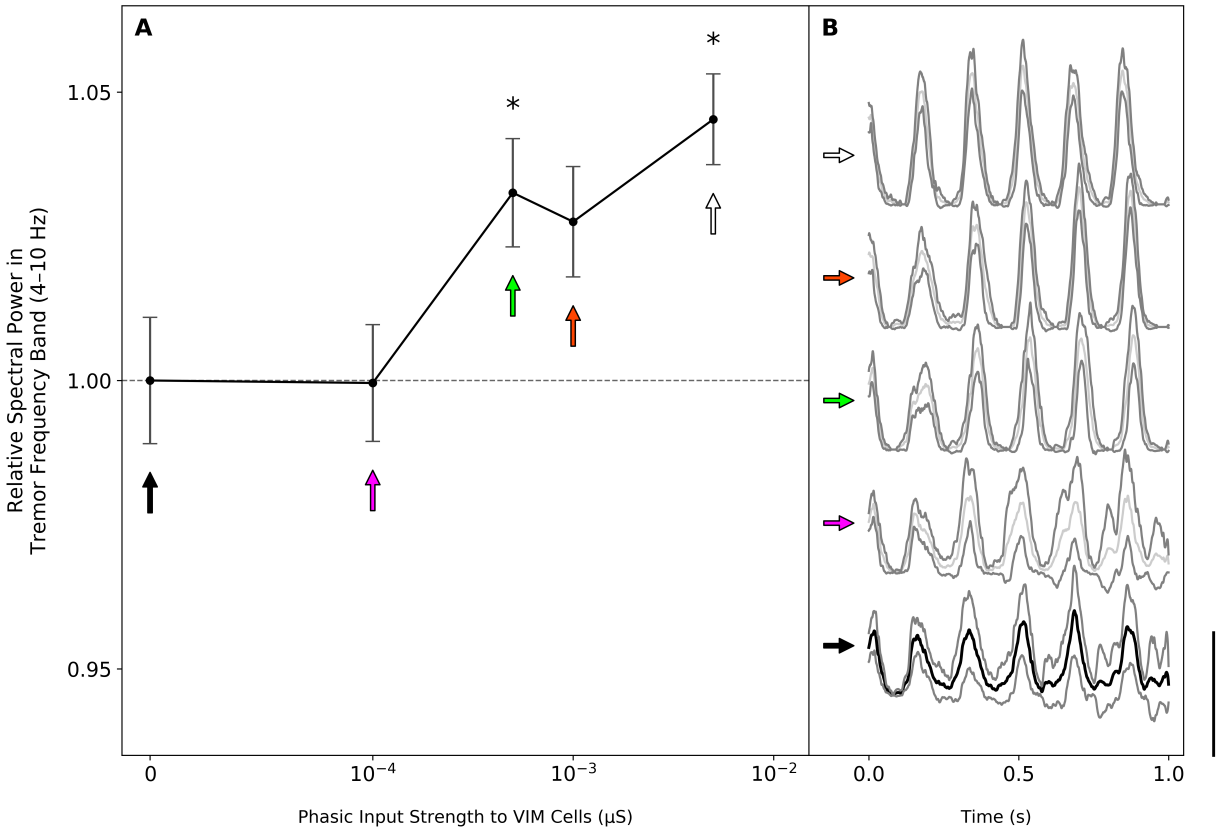

Figure 8: **Intrinsic network tremor frequency power increased with tremor-phasic input.** Phasic, 6 Hz synaptic inputs onto the VIM cells increased the tremor spectral power of intrinsically generated tremor oscillations. Values in Table 4A. A. Increased strengths of phasic input increased tremor activity with ongoing intrinsic oscillations. B. Mean spike histograms for simulations at each value of input. Arrows correspond to points in (A). Dark black line denotes mean intrinsic tremor in the absence of additional inputs. Gray lines are standard error. Scale bar is 25 sp/s.

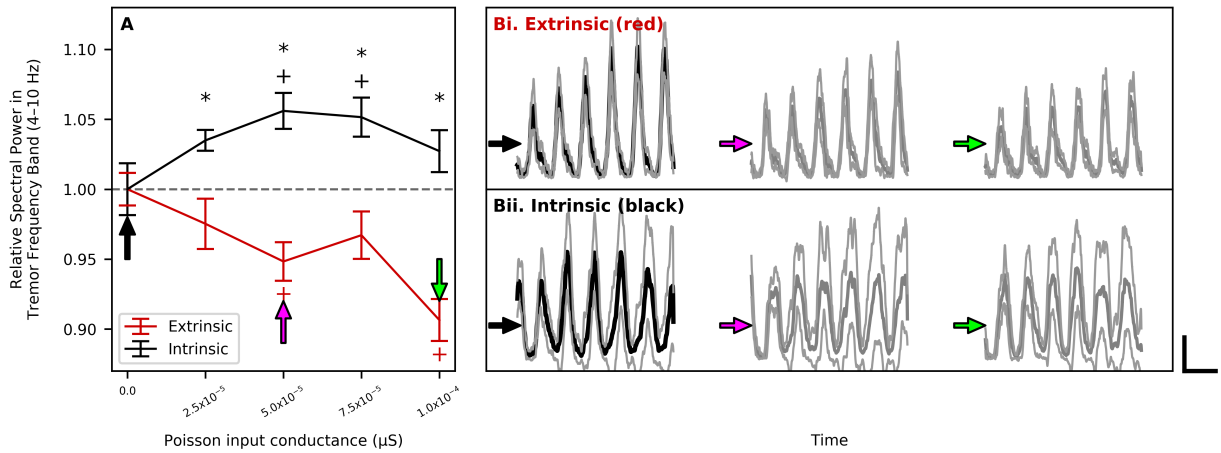

Figure 9: **Non-tremor frequency inputs increased intrinsic but not extrinsic tremor frequency activity.** An AMPA-ergic Poisson-distributed input was simulated as a model of non-tremor motor activity from cerebellum or cortex. Scale bars for B are 0.2 s and 5 sp/s. Values in Table 4B. A. The tremor frequency power relative to the baseline was tracked as the input conductance was increased for both the extrinsic (red) and intrinsic (black) model networks. As the input conductance increased, tremor frequency power in the extrinsic network was significantly reduced from baseline (red +), and the tremor frequency power in the intrinsic network was significantly increased from baseline (black +). For the same input, tremor frequency power was significantly greater in the intrinsic network compared to the extrinsic network (black asterisks). Values for the conductances and spectral power in Table 4. Bi. Mean VIM cell spike convolutions for the intrinsic network are shown for 3 input strengths. While the Poisson input did not increase the overall amplitude, the shape of the activity was more sinusoidal, leading to increases in power. Colors corresponded to A. Bii. Mean VIM cell spike convolutions for the extrinsic network are shown for 3 input strengths. The Poisson input interfered with the tremor-periodic input driving the extrinsic activity, reducing the overall amplitude. Colors corresponded to A.